Review

Azizeh-Mitra Yousefi*, Hassane Oudadesse, Rosa Akbarzadeh, Eric Wers and Anita Lucas-Girot

Physical and biological characteristics of nanohydroxyapatite and bioactive glasses used for bone tissue engineering

Abstract: Critical-sized bone defects have, in many cases, posed challenges to the current gold standard treatments. Bioactive glasses are reported to be able to stimulate more bone regeneration than other bioactive ceramics; however, the difficulty in producing porous scaffolds made of bioactive glasses has limited their extensive use in bone regeneration. On the other hand, calcium phosphate ceramics such as synthetic hydroxyapatite and tricalcium phosphate are widely used in the clinic, but they stimulate less bone regeneration. This paper gives an overview of the recent developments in the field of bioactive nanoparticles, with a focus on nanohydroxyapatite and bioactive glasses for bone repair and regeneration. First, a brief overview of the chemical structure and common methods used to produce synthetic nanohydroxyapatite and bioactive glasses has been presented. The main body of the paper covers the physical and biological properties of these biomaterials, as well as their composites with biodegradable polymers used in bone regeneration. A summary of existing challenges and some recommendations for future directions have been brought in the concluding section of this paper.

Keywords: 3D scaffold; Bioglass® 45S5; bone tissue engineering; hydroxyapatite; nanoparticles.

DOI 10.1515/ntrev-2014-0013
Received June 17, 2014; accepted July 28, 2014; previously published online September 16, 2014

***Corresponding author: Azizeh-Mitra Yousefi,** Department of Chemical, Paper and Biomedical Engineering, Miami University, Oxford, OH 45056, USA, e-mail: yousefiam@MiamiOH.edu
Hassane Oudadesse, Eric Wers and Anita Lucas-Girot: University of Rennes 1, UMR CNRS 6226, 263, av. Du Général Leclerc, 35042 Rennes, France
Rosa Akbarzadeh: Department of Chemical, Paper and Biomedical Engineering, Miami University, Oxford, OH 45056, USA

1 Introduction

Nanotechnology has shown promise in universally improving all materials used for bone regeneration through either constituent nanomaterials or nanostructured surface features. Nanomaterials possess superior properties compared to their micron-structured counterparts [1]. Therefore, nanotechnology involves understanding and controlling matter on the nanometer scale, where unique phenomena enable new functional applications [2]. Among nanomaterials, nanohydroxyapatite (n-HA) has been widely used in scaffolds for bone tissue engineering as well as implant coating material. The quality of a coating is highly dependent on the overall characteristics and attributes of the synthesized powders. Such attributes include density, purity, phase composition, crystallinity, particle size, particle-size distribution, particle morphology, and specific surface area [3]. These factors determine the resulting success of the HA coating deposited onto orthopedic implants. Therefore, the recent trend is focused on improving the mechanical and biological properties of bioceramics using nanotechnology [3].

Critical-sized bone defects caused by tumor resection, trauma, or selective surgery have, in many cases, posed challenges to the current gold standard treatments [4]. The repair rate of a bone defect is dependent on the wound size [5]. When the defect size is greater than the healing capacity of osteogenic tissues, the fibrous connective tissue regenerates faster than bone tissue and becomes dominant in the bone defect [6]. Being a native component of bone, n-HA has an ability to promote mineralization and is a common choice as a bone graft substitute and bone filler material [7]. Nanocomposites that combine n-HA with a biodegradable polymer can capture the benefits of both components. While biodegradable polymers such as poly(lactic-co-glycolic acid)(PLGA) offer tunable degradation rates and ease of processing, the

n-HA component within polymer matrix can increase the overall mechanical strength of the composite due to the high compressive modulus and hardness of n-HA. Moreover, the presence of n-HA can enhance bone cell response, slow down the degradation rate, and mediate the pH drop induced by the acidic degradation products of PLGA [8].

The development of artificial nanostructures to replicate the complex nanoscale features of biological tissues (e.g., bone) can lead to promising biomaterials [9]. Nanotechnology approach to regenerative medicine sounds obvious when examining nature. For example, bone is a nanocomposite composed of a protein-based soft hydrogel template (i.e., collagen, water, and noncollagenous proteins such as laminin, fibronectin, and vitronectin) and hard inorganic components made of n-HA [10]. The nanocrystalline HA in the bone matrix is typically 20–80 nm long and 2–5 nm thick. The protein components in the bone extracellular matrix (ECM) are also nanometer in dimension [10]. Figure 1 shows the dimensional principles of bone construction, where nanoscale bundles of protein act as a template for the crystallization of HA nanocrystals.

To replicate the extraordinary strength and durability of natural bone, the current trend is to design biomaterials that nearly mimic bone in terms of its structural levels of organization from the nanoscale upward [10]. Figure 2 shows some of the advantages of biomimetic nanomaterials. For example, the self-assembled nanostructured ECM in bone (Figure 2A) closely surrounds and affects the adhesion, proliferation, and differentiation of mesenchymal stem cells (MSC), osteoblasts (bone-forming cell), osteoclasts, and fibroblasts. Novel nanomaterials that possess excellent mechanical properties, while being biomimetic in terms of their nanostructure, have shown promise in designing implants and tissue engineering scaffolds (Figure 2B). Nanostructured materials with surface properties favoring cell adhesion have a greater chance of stimulating new bone growth compared to conventional materials (Figure 2C). This is one of the underlying mechanisms that make nanomaterials superior to conventional materials for tissue engineering applications [10].

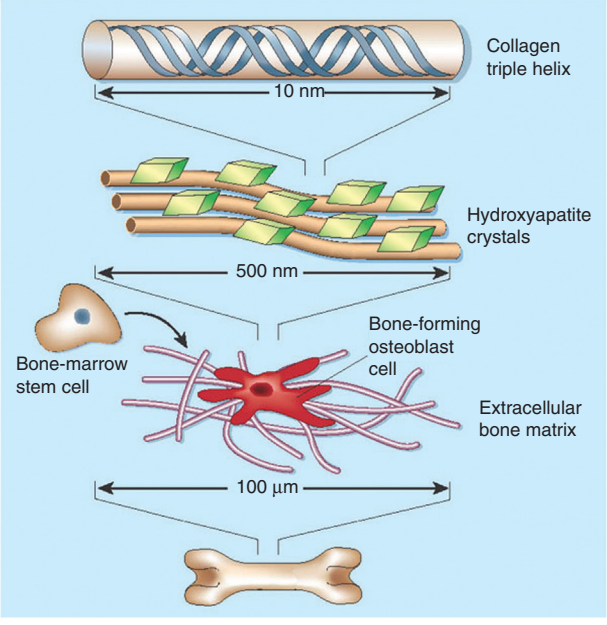

Figure 1 Nanoscale bundles of protein, composed of collagen triple helices, act as a template for the crystallization of hydroxyapatite nanocrystals. Reprinted with permission from Ref. [9]. Copyright © 2001 Nature Publishing Group.

In the past two decades, there has been a continuous increase in research efforts aiming to develop engineered structures with improved mechanical properties, by taking advantage of the inherent high surface area/volume ratio of nanoparticles [11]. This paper gives an overview of the application of inorganic nanoparticles in biomedical fields, with a focus on hydroxyapatite and bioactive glass nanoparticles for bone tissue engineering. First, a brief overview of the chemical structure and some common methods used to produce synthetic hydroxyapatite and bioactive glasses has been presented (in their respective sections). The main body of the paper covers the physical and biological properties of these biomaterials, as well as their composites with biodegradable polymers used in bone regeneration. A summary of existing challenges and some recommendations for future directions have been brought in the concluding section of this paper.

2 Nanohydroxyapatite

2.1 Chemical structure

Hydroxyapatite (HA), $Ca_{10}(PO_4)_6(OH)_2$, is the basic mineral constituent of human bone and tooth enamel. The stoichiometric HA contains calcium (Ca) and phosphorus (P) at a molar ratio of 1.67 (Ca/P). However, HA in human bones is usually nonstoichiometric due to Ca deficiency with Ca/P ratios varying from 1.5 to 1.67, which affects the biological and mechanical properties of HA [12]. The HA crystal consists of tightly bonded PO_4 tetrahedral units, two types of Ca atoms, and OH groups. As shown in Figure 3, four Ca1 atoms are coordinated with three oxygen (O) ions forming triangles, whereas six Ca2 atoms are coordinated with six oxygen atoms and one OH group [12]. Ca1 and Ca2 are

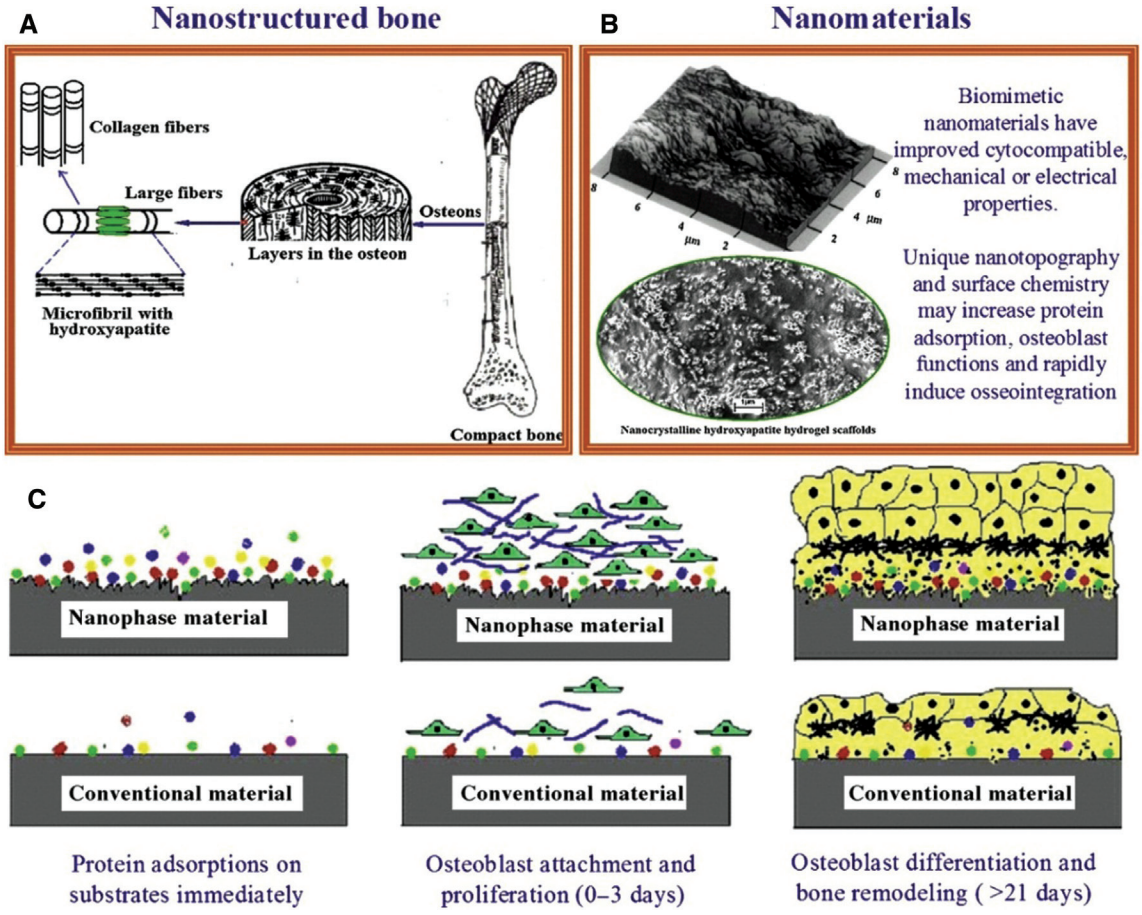

Figure 2 (A) The nanostructured hierarchical self-assembly of bone. (B) Nanophase titanium (top, the atomic force microscopy image) and a nanocrystalline hydroxyapatite hydrogel scaffold (bottom, the scanning electron microscopy image). (C) Schematics of the mechanism by which nanomaterials tend to be superior to conventional materials for bone regeneration. The bioactive surfaces of nanophase materials mimic those of native bone and promote protein adsorption and stimulate more new bone formation than conventional materials. Reprinted with permission from Ref. [10]. Copyright © 2009 Elsevier.

columnar Ca and axial Ca, respectively, and represent two nonequivalent crystallographic sites. Slight imbalance in stoichiometric Ca/P ratio in HA (from the standard value of 1.67) can lead to the formation of either α- or β-tricalcium phosphate upon heat treatment. However, it should be possible to sinter stoichiometric HA without running into purity issues, at temperatures in excess of 1300°C [13].

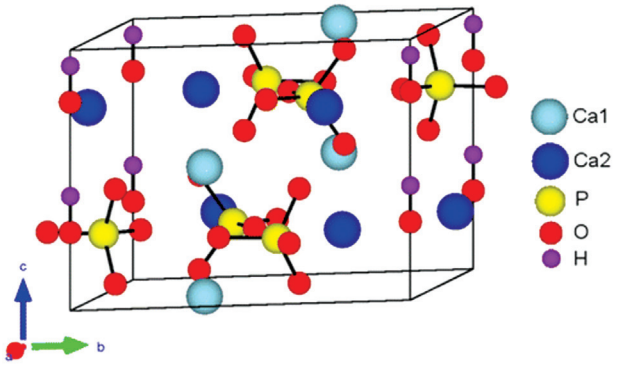

Figure 3 Hexagonal unit cell of stoichiometric hydroxyapatite. Reprinted with permission from Ref. [12]. Copyright © 2014 American Chemical Society.

The degradation time of amorphous HA is much shorter than that of crystalline HA [1]. In general, amorphous HA can form as a precursor phase in a solution at sufficiently high supersaturation and pH. Subsequently, it transforms to the thermodynamically stable HA [$Ca_{10}(PO_4)_6(HO)_2$] [14]. The degradation rate of HA also depends on its particle size. Nanocrystalline calcium phosphates degrade faster than micron (or conventional) grain size calcium phosphates. Nanocrystalline HA exhibits improved sinterability and enhanced densification due to greater surface area, which may improve fracture toughness as well as other mechanical properties [15]. It should be mentioned that calcium phosphate compounds with Ca/P ratio of <1:1 are not suitable for

biological implantation. This is due to their increased solubility and speed of hydrolysis with decreasing Ca/P ratio [13].

2.2 Synthesis

Hydroxyapatite (HA) can be synthesized by a variety of methods such as hydrothermal [16, 17], sol-gel [17–20], wet chemical [3, 21], biomimetic deposition [22, 23], solid-state reaction [24], and microbial method [25]. It is important to carefully control the operating condition during the synthesis, including pH, reaction time, temperature, concentration of the reactants, as well as the proper selection of the precursor materials [26]. This is because these parameters and materials can significantly affect the composition and properties of the final HA product [27]. Table 1 briefly compares some of the common methods to synthesize HA and provides the typical operating condition and the characteristics of the synthesized product.

The hydrothermal method allows for the formation of well-crystallized HA powder. In this method, the synthesis is performed in the presence of water at a relatively high temperature and pressure. Heating the reactants in a sealed container leads to an autogenously pressurized system as the temperature rises [26]. Conversely, the sol-gel process can generate apatite crystals at low temperatures and pressures due to high reactivity of the reactants [18]. This method also improves the chemical homogeneity of the final HA product because it involves mixing of calcium and phosphorus in the molecular level. The main disadvantage of the sol-gel method is the long time it takes to gel HA, although this issue can be resolved by performing the reaction at higher temperatures and pressures [26]. In addition, sol-gel powders require calcination at high temperature in the presence of air to produce crystalline products [17].

The wet chemical precipitation carried out at atmospheric conditions is another simple and convenient method for synthesizing HA powder [21]. The shape, size, and surface area of the HA obtained using the wet chemical precipitation are highly sensitive to the reaction rate and temperature [26]. The main difference between the sol-gel and wet chemical methods is that the former involves gelation of the whole reactant mixture, whereas the latter involves precipitation of HA solids with the product remaining in the aqueous phase. As for the biomimetic deposition method, it has been shown that chemical precipitation of calcium nitrate tetrahydrate and diammonium hydrogen phosphate salts, dissolved in simulated body fluid (SBF) solutions at 37°C and pH of 7.4, can produce homogeneous and pure ceramic powder [22]. In this process, the SBF can facilitate the growth and generation of bone-like calcium apatite on immersed materials such as bioactive glasses and silica gel samples at a physiological pH and temperature [26].

2.3 Physical properties

The low tensile strength and brittleness limit the use of ceramics in biomedical applications, where they can be exposed to significant torsion, bending, or shear stress [28–30]. Hydroxyapatite scaffolds hardly remodel with time [31] and do not change shape in response to physiological loads; therefore, they cannot grow with the patient. In addition, the uncontrolled *in vivo* degradation of ceramics (e.g., β-tricalcium phosphate, β-TCP) may increase extracellular concentrations of calcium and phosphate ions, trigger cell death, and cause adverse side effects [28, 32]. To overcome these shortcomings, many studies have looked into developing polymer/ceramic composite scaffolds [33–37]. The rationale is to combine the benefits of cell interactions and enhanced mineralization of ceramics [8, 38, 39], with the topology control, ease of processing, and desirable mechanical strength of synthetic materials [40].

Table 1 Methods to synthesize hydroxyapatite. Modified from Ref. [26].

Method	Properties	Operating condition	Characteristic of HA produced
Hydrothermal	Reaction is conducted at a relatively high pressure in the presence of water	Temperature range of 80°C–400°C and pressure at 100 MPa	HA whiskers with 20–30 μm length and 0.1–1 μm width
Sol-gel	Involves the molecular level mixing of calcium and phosphorus featuring high reactivity	Temperature range of 65°C–600°C	HA nanoparticles with 20–50 nm diameter
Wet chemical	Involves a simple setup, low operating temperature, as well as high production of pure product	Typical temperature of 140°C and pressure of 0.3 MPa	HA with biphasic rod-like structure
Biomimetic deposition	Nucleation and growth of HA are promoted by simulated body fluid (SBF)	Temperature of 37°C	Bone-like apatite layer of HA is formed

Composite organic/inorganic materials could allow combining the tunable degradation rate and high release efficiency of polymers with the osteoconductivity and delayed/sustained release characteristics of ceramic materials [41]. Another advantage of polymer/ceramic composites is that the acidic degradation by-products from polyesters can be buffered in the presence of ceramics [39]. Therefore, carefully designed composites of bioactive ceramics and biodegradable polymers may offer adequate mechanical property, desired biocompatibility, and resorption rate, as well as improved tissue interaction and osteoconductivity [28]. The following subsections give an overview of the effect of HA nanoparticles on the surface properties, mechanical properties, and degradation rate of biomaterials.

2.3.1 Surface characteristics

It is well known that the physicochemical parameters of the biomaterial surface (e.g., surface energy, surface charges, or chemical composition) affect cell responses [42], while mediating the adsorption of specific proteins such as fibronectin, vitronectin, and laminin [10]. For example, extracellular matrix protein adsorption onto biomaterial surface, and subsequent modulation of cell adhesion, is highly affected by surface energy [43]. Therefore, a classical approach to altering cell interactions with biomaterial is changing its surface energy or wettability (i.e., hydrophilicity/hydrophobicity) [43]. Biomaterial surface composition and roughness, immobilization of various chemical agents to the surface, and the presence of nanofeatures on the surface can alter the surface wettability [44]. Surface wettability has been traditionally quantified by water contact angles (θ), which is closely related to surface energy according to the Young-Dupré equation [45]:

$$\cos\theta=(\gamma_{sv}-\gamma_{sl})/\gamma_{lv}$$

where γ_{sv} is the surface energy of the solid, γ_{sl} is the solid-liquid interfacial tension, and γ_{lv} is the surface tension of the liquid. In general, water contact angle of <65° is considered as a hydrophilic characteristic for a surface [46, 47]. Hydrophobicity of micro- and nano-patterned surfaces could be dependent on their structural morphology as well as surface chemistry [48]. Figure 4 shows the scanning electron microscopy (SEM) images of nano- and micro-patterned morphologies on stainless steel. The change in water contact angle suggests an enhanced hydrophobicity with increasing the feature size.

Contact angle measurement has been used to investigate the effect of n-HA on surface wettability of polymeric scaffolds produced by electrospinning [49–51]. Ngiam et al. [50] used calcium and phosphate (Ca-P) solution dipping method to form n-HA on PLGA and PLGA/collagen (Col) nanofibers. Figure 5 shows that incorporation of n-HA into PLGA (θ: 107.5°±1) significantly increased the hydrophobicity of pure PLGA (θ: 75.9°±4.9) nanofibers [50]. Conversely, the presence of n-HA improved the hydrophilicity of the PLGA/Col+n-HA (θ: 11.2°±2.7) scaffolds, in comparison with pure collagen (54.6°±8.7) and collagen/PLGA (29.1°±3.4) nanofibers. The -COOH functional groups of collagen enhanced the hydrophilic characteristics of the nanofibers. In addition, the types of functional groups present in collagen, i.e., scilicet carboxyl groups and carbonyl groups, served as nucleation sites for apatite formation and led to uniform distribution of n-HA on the outer and inner surfaces of the PLGA/Col nanofibers [50]. This could explain the decrease in contact angle for PLGA/Col+n-HA scaffolds, compared to that of PLGA+n-HA. Direct relationship has been reported between the high surface energy of hydrophilic nanomaterials and the adsorption of hydrophilic cell adhesive proteins [52]. In light of this, it has been speculated that hydrophilic

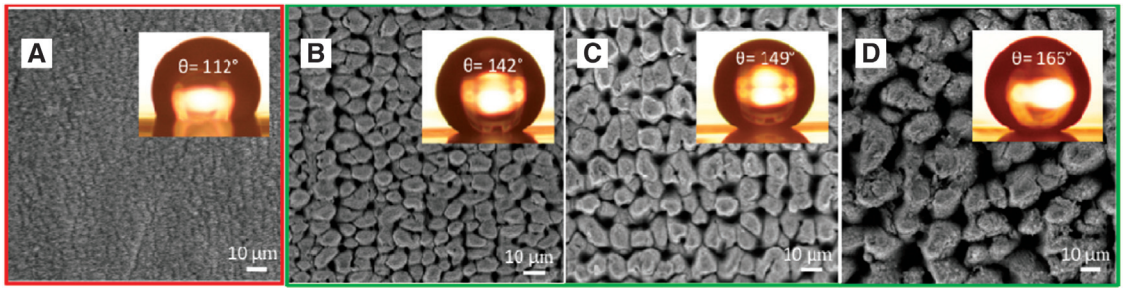

Figure 4 SEM images showing the change in water contact angle for different nano/micro-patterns on stainless steel. Reprinted with permission from Ref. [48]. Copyright © 2013 IOP Publishing.

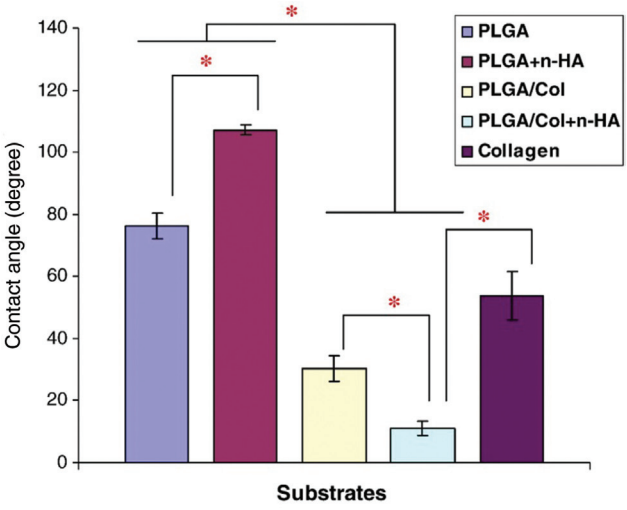

Figure 5 Hydrophilicity of different nanofiber formulations. Reprinted with permission from Ref. [50]. Copyright © 2009 Elsevier.

nanomaterials have a higher affinity for such cell adhesive proteins and, subsequently, they could enhance cell functions better than hydrophobic nanomaterials [52, 53].

The growing interest in nanomaterials for tissue-engineering applications primarily lies on their unique surface energies, which appears to be a stronger rationale than the ability of nanomaterials to mimic dimensions of tissue components [54]. Surface analysis of tissue engineering scaffolds has indicated that the addition of n-HA filler may lead to an increase in surface oxygen and enhanced surface energy [55]. Luong et al. [56] modified the surface of electrospun poly(L-lactic acid) (PLLA) fibers by incorporating HA nanocrystals (30 nm in diameter and 100–120 nm in length). The modified fibers revealed a higher surface energy, lower water contact angle, improved hydrophilicity, and enhanced cell attachment.

2.3.2 Mechanical properties

An important factor in bone tissue engineering is the choice of scaffold architecture and composition, enabling adequate mechanical properties to withstand dynamic remodeling of the engineered bone under *in vivo* conditions. An ideal scaffold should be mechanically stable while providing a highly porous architecture with interconnected pore network [57]. In general, the stiffness and compressive strength of common polymeric scaffolds are insufficient compared to those of human bone. Therefore, organic/inorganic composite structures have been widely used to enhance and modulate the mechanical properties of bone scaffolds. These organic/inorganic systems aim to mimic the composite nature of native bone by combining the toughness of polymer phase with the compressive strength of the inorganic component [11].

Table 2 gives a summary of the mechanical properties and porosity of human bone [58]. The hierarchical structure of bone contributes to its unique mechanical properties. For example, the toughness of bone is achieved by the interplay of organic collagen network that supports the inorganic mineral phase [59]. Given the low mechanical properties of collagen-based scaffolds, many studies have combined collagen with calcium phosphates to develop biomimetic scaffolds with improved mechanical properties [50, 60, 61]. Micron-sized HA (m-HA) particles can lead to poor resorbability and brittle constructs. However, incorporating nano-sized HA (n-HA) into porous collagen scaffolds has shown to produce biocomposite scaffolds with improved resorbability and mechanical characteristics [60]. Similarly, the interaction between nano-scale components and a polymer matrix is the basis for enhanced mechanical and functional properties of nanocomposite scaffolds.

The mechanical properties of composites are controlled by microstructural parameters such as the properties of the matrix, properties and distribution of the fillers, as well as the interfacial bonding and the synthesis or processing methods [11]. For example, a combination of well-dispersed nanoceramics in PLGA has shown to enhance the compressive modulus, tensile modulus, tensile strength at yield, and ultimate tensile strength compared with more agglomerated nanoceramics in PLGA [62]. Therefore, the polymer/filler interfaces may affect the effectiveness of load transfer between the composite constituents. Surface modification of nanostructures has been proposed to promote better dispersion of particles and to enhance interfacial adhesion [11].

Table 2 Summary of the mechanical properties and porosity of human bone. Reprinted with permission from Ref. [58]. Copyright © 2011 Elsevier.

	Compressive strength (MPa)	Flexural strength (MPa)	Tensile strength (MPa)	Modulus (GPa)	Porosity (%)
Cortical bone	130–180	135–193	50–151	12–18	5–13
Cancellous bone	4–12	–	1–5	0.1–0.5	30–90

Roohani-Esfahani et al. [63] developed a composite biphasic calcium phosphate (BCP) scaffold by coating a nanocomposite layer, consisting of n-HA and PCL, over the surface of BCP. The effects of HA particle size and shape in the coating layer on the mechanical properties of the BCP scaffolds were examined. The compressive strength of the scaffolds coated with needle-shape n-HA-composite (2.1±0.17 MPa) was considerably higher than that of micro-HA (m-HA)-composite coated scaffolds (0.29±0.07 MPa). This was attributed to the high interfacial bonding between n-HA particles and PCL, as well as to the nanocomposite layer that was well bonded to the surface of the scaffold even at the breaking point [63].

Zhang et al. [64] investigated the mechanical properties of dense n-HA/PLLA composites prepared by a modified *in situ* precipitation method, using $Ca(OH)_2$ and H_3PO_4 as precursors for the synthesis of HA phase. When the HA content increased from 0 to 20 wt%, the compressive strength of the composites increased monotonically from 53 to 155 MPa. The Young's modulus showed a comparable increase from 1.2 to 3.6 GPa. These values were higher than those of the samples prepared by direct mixing. The results listed in Table 3 suggest that the n-HA/PLLA composites prepared by the *in situ* precipitation had superior mechanical properties than those of n-HA/PLLA composites reported in the literature [65–67]. The modified *in situ* precipitation method was found to resolve the aggregation problem of the nano-sized particles in the polymer matrix. From Table 3, it could also be concluded that increasing the molecular weight of the polymer could enhance the mechanical properties. However, increasing the HA content might decrease the strength in some cases, possibly due to the aggregation of nanoparticles.

Wagoner Johnson and Herschler have reviewed the compressive, flexural, and tensile properties of calcium phosphates (CaPs) and CaP/polymer composites for applications in bone replacement and repair [58]. This includes HA particles, as one of the major components of the native bone environment. Figure 6 shows the data for the studies in which the HA content varied in HA/polymer composites [33, 34, 36–58, 67–69]. An interesting observation is that the addition of HA does not seem to increase strength over that of the monolithic polymer in most of the reported cases. As some researchers add the harder HA phase to the polymer scaffolds in order to increase strength, these compiled data show minimal effect or the opposite of what is intended in these studies. The discrepancy between the results presented in Figure 6 and findings of Zhang et al. [64] in Table 3 could be due to differences in experimental methods used in these studies (e.g., agglomeration of nanoparticles).

2.3.3 Degradation rate

Biomaterials used in tissue engineering scaffolds should stimulate and support tissue ingrowth, withstand the loading conditions experienced *in situ*, while degrading with a comparable rate at which new tissue forms. The degradation kinetics of a biomaterial may affect a range of processes such as host response, cell growth, and tissue regeneration [11]. Synthetic biopolymer-based nanocomposites are of great interest as scaffold materials for tissue engineering due to their adjustable biodegradation kinetics and biocompatibility [70]. As mentioned earlier, for such composites, the alkalinity of inorganic particles (e.g., HA) neutralizes acidic autocatalytic degradation of polymers such as poly(L-lactic acid) (PLLA) [11].

Figure 7 shows the schematics of the biodegradation process, where the factors affecting the degradation are highlighted and correlated to their importance in biomedical application [11]. Incorporation of nanostructures to biodegradable polymers can alter their degradation behavior, by allowing rapid exchange of protons in

Table 3 Compressive strength and Young's modulus of dense HA/PLLA composites. Modified from Ref. [64].

Investigators	Tested material			Mechanical properties	
	Molecular weight of PLLA (kDa)	HA characteristics (content, size)	Processing conditions	Compressive strength (MPa)	Elastic modulus (GPa)
Zhang et al. [64]	200	10 wt%, 40–100 nm	145°C, 200 MPa	109±8	2.3±0.2
		20 wt%, 40–100 nm		155±8	3.6±0.2
Gay et al. [65]	104	25 wt%, 100 nm	190°C, 300 MPa	88	3.8
		50 wt%, 70–100 nm		97	5.6
Ignjatovic et al. [66]	100	80 wt%, 0.5–0.7 nm	176°C, 98 MPa	38	2.0
		80 wt%, 100 nm		72	3.5
Shikinami et al. [67]	202	50 wt%, 0.3–20 nm	103°C	115	6.5

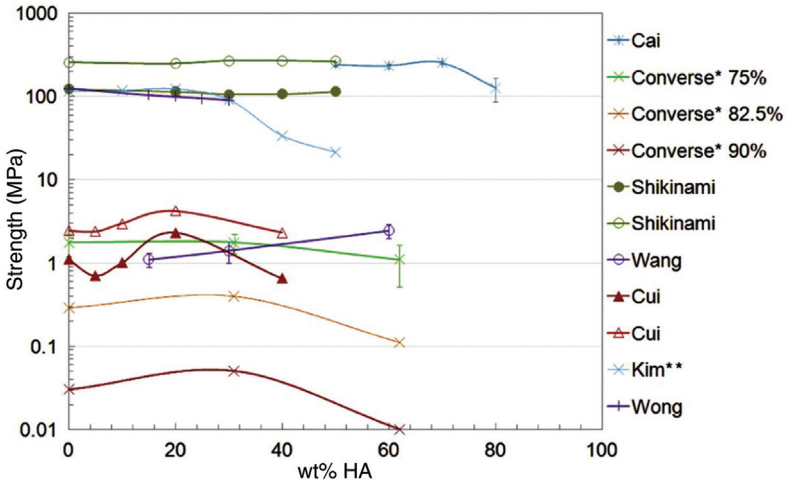

Figure 6 Data illustrating the effect of wt% HA on the strength of HA/polymer composites [33, 34, 36, 37, 58, 67–69]. Data in this review were averaged and represented with error bars in cases in which there were multiple test conditions for a given fraction of HA. *Data from Converse et al. were converted from vol% to wt% by the authors of the review. **Kim et al. used calcium silicate rather than HA. Reprinted with permission from Ref. [58]. Copyright © 2011 Elsevier.

water for alkali in a ceramic. Therefore, composite materials based on inorganic nanoparticles have shown an enhanced polymer degradation rate if compared to pure polymers, due to both biodegradation mechanism of the polymers and dissolution of nanoparticles [11]. Tunable degradation rates and superior bioactivity make these nanocomposites promising materials for tissue engineering applications.

Kim et al. [71] coated HA porous scaffolds with HA-PCL composites and entrapped an antibiotic drug within the coating layer. With manipulating the coating concentration and HA/PCL ratio, the mechanical properties, morphology, and biodegradation behavior of these constructs were investigated. The rate of *in vitro* biodegradation of the composite coatings in the phosphate-buffered saline (PBS) solution differed with the coating concentration and HA/PCL ratio, where the higher concentration and HA content increased the biodegradation [71].

Roohani-Esfahani et al. [63] investigated the effect of the shape and size of HA particles on the bioactivity of the BCP composite scaffolds coated with HA/PCL composites. The scaffolds coated with n-HA/PCL composites showed slower dissolution rates and superior bioactivity compared to those coated with either m-HA/PCL composites or polymer-only [63]. These results were in contrast with other studies on the role of HA particles on degradation of composite layer, including the findings of Kim et al. [71], where adding m-HA particles into PCL increased the degradation rate due to increased water absorption. As HA contains hydroxyl group, it can act as a catalyst for hydrolytic decomposition of PCL [72]. The contradictory findings reported by Roohani-Esfahani were attributed to the complex nature of degradation process in polymer/HA composites [63].

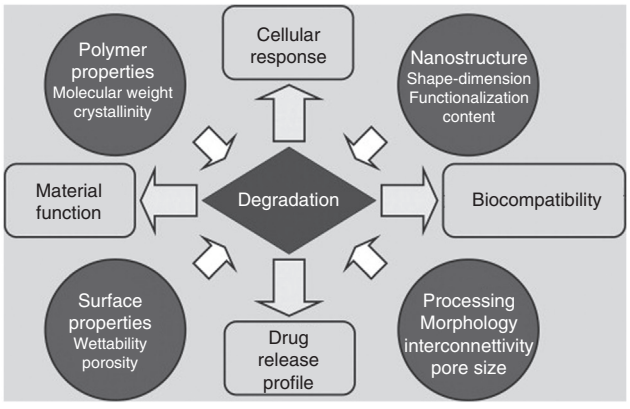

Figure 7 Importance of biodegradability in biomedical application. Reprinted with permission from Ref. [11]. Copyright © 2010 Elsevier.

2.4 Biological properties

Calcium phosphate ceramics such as HA and tricalcium phosphate (TCP) have a chemistry similar to the mineral phase of natural bone. As a result, their reaction with physiological fluids forms strong bonds to hard and soft tissues, thereby increasing osteointegration. The nanoscale feature of n-HA induces advantageous cellular responses when compared with m-HA [7]. This is because the surface topography of a biomaterial is one of the most crucial physical cues for cells. Both nanotopography and microtopography can modulate cell behavior such as cell adhesion,

differentiation, and proliferation [42]. Studies have shown that nanostructured surfaces promote greater amounts of specific protein interactions and, more efficiently, stimulate new bone formation. This may be one of the underlying mechanisms for superior tissue growth observed for nanostructured biomaterials. This has led to the design of various nanophase ceramic, polymer, metal, and composite scaffolds for tissue engineering applications [10].

Webster et al. [73] reported that 67-nm HA particles significantly enhanced osteoblast adhesion, compared to conventional 179-nm HA particles after just 4 h of culture, while strikingly inhibiting competitive fibroblast adhesion. Nanophase ceramics have demonstrated the highest adsorption of vitronectin, which is a protein that promotes osteoblast adhesion. Moreover, enhanced osteoclast-like cell functions and the formation of resorption pits have been observed on n-HA compared to conventional HA [10]. In light of this, n-HA is expected to have better bioactivity compared to coarser crystals and has been used for engineered tissue implants with improved biocompatibility [74].

Cai et al. [75] investigated the effect of n-HA particles, typically 20±5, 40±10, and 80±12 nm in diameter, on the proliferation of bone marrow mesenchymal stem cells (MSCs). The *in vitro* cell culture trials showed improved cytophilicity of the nanoparticles compared with conventional HA (typically rod-like with a width of 30–80 nm and a length of 200–500 nm). Greater proliferation of MSCs and cell viability were measured on the n-HA particles, particularly for 20-nm-sized particles. It was concluded that the particle size could play a key role in replacement and reconstruction of bone, especially after partial ablation of bone tumors [75]. An *in vivo* study in a sheep model has shown that n-HA-coated metallic (Ti6Al4 V) screws can enhance fixation and provide superior stabilization, bone ingrowth, and osteointegration compared with m-HA-coated screws [76]. In light of the reported studies, nano-HA particles (n-HA) have demonstrated distinct regenerative advantages when compared with micron-sized particles (m-HA). This has been a driving factor in the development of composite scaffolds optimized to promote rapid osteogenesis *in vivo* [38].

There have been extensive studies on the effect of HA particle characteristics (size, shape, and sintering temperature) on biological responses and on the production of various inflammatory cytokines. Needle-shaped microparticles have been found to induce the highest production of inflammatory cytokines [77–79]. Cai et al. [75] reported that the cytotoxic effect of n-HA on MSCs was dependent on their size and ζ potential values. Zhao et al. [79] demonstrated that higher particle-cell association and increased cellular uptake of n-HA need not lead to increased cytotoxicity, indicating the role of particle shape in toxicity. Further analysis looking into intracellular dissolution and cellular uptake mechanisms will be vital in order to understand the mechanisms by which cells detect and respond to n-HA [79, 80].

Xu et al. [80] compared the effect of four types of n-HA with different nanocrystal morphologies and sizes on growth inhibition and apoptosis in primary cultured rat osteoblasts. The study included needle-shaped (10–20 nm in diameter and 30–50 nm in length), spherical (10–30 nm in diameter), long rod-like (20–40 nm in diameter and 200–400 nm in length), and short rod-like (20–40 nm in diameter and 70–90 nm in length) crystals. The osteoblasts were treated with the four types of n-HA at various concentrations (20, 40, 60, 80, or 100 mg l^{-1}). It was reported that the higher the n-HA concentration, between 20 and 100 mg l^{-1}, the stronger the toxicity (Figure 8) [80]. Most of the cytotoxicity was attributed to apoptosis rather than necrosis. At the same concentration, n-HA with smaller surface areas produced lower apoptosis rates, suggesting the potential morphology-driven cytotoxic effects of n-HA on osteoblasts [80].

3 Bioactive glasses

3.1 Chemical composition

Glass is an amorphous solid without long-range order in its structure. The oxides used to synthesize glass are

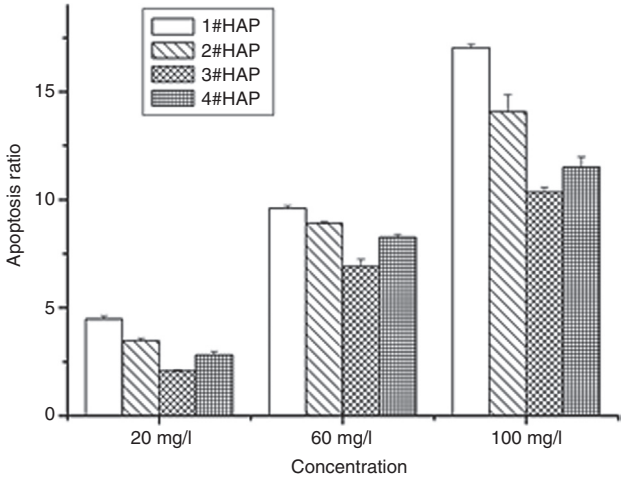

Figure 8 Hydroxyapatite nanoparticles inducing apoptosis in osteoblasts; (1) needle-shaped, (2) spherical, (3) long rod-like, (4) short rod-like. Reprinted with permission from Ref. [80]. Copyright © 2010 John Wiley and Sons.

classified into three groups according to their functions: (i) network-forming oxides (e.g., SiO_2 and P_2O_5); (ii) network-modifying oxides (e.g., CaO and Na_2O); and (iii) intermediate oxides (e.g., ZnO and Al_2O_3). Network-forming oxides are composed of metallic elements, which can form multiple chemical bonds with the oxygen atoms. These oxides form polyhedrons that are tied by their peaks and give rise to the vitreous network. Network-modifying oxides are composed of alkaline and alkaline-earth elements. The introduction of alkaline elements forms discontinuities in the vitreous network and decreases the viscosity of a glass [81]. Moreover, alkaline oxides (e.g., Na_2O) sharply reduce the glass transition temperature of a glass [82], whereas alkaline-earth oxides (e.g., CaO) have a lower impact on the glass transition temperature [83]. The principal intermediate elements in glass oxides are Al, Fe, Ti, Ni, and Zn [84, 85]. The presence of certain metal elements results in modifications of the thermal behavior of the glass. For example, molybdenum (Mo) introduced in the matrix of silicate-phosphate glasses can reduce the glass transition temperature, the specific heat, and the thermal stability [86].

Bioactive glasses and glass-ceramics are special compositions made typically from Na_2O-CaO-MgO-P_2O_5-SiO_2 systems (Table 4) [87]. A bioactive material is defined as a material that stimulates a beneficial response from the body, particularly bonding to host tissue (usually bone) [88]. The discovery of bioactive glasses dates back to 1969 [87], when a special composition of soda-lime-phosphate-silicate glass was made by Hench et al. [89], and its bonding to bone was reported in peer-reviewed publications [89–91]. Three important compositional features of this glass distinguished it from traditional soda-lime- silica glasses: <60 mol% SiO_2, high Na_2O, and CaO content, and high CaO:P_2O_5 ratio. These compositional features make the surface highly reactive when exposed to body fluids [92].

Before the discovery of bioactive glasses, the initial emphasis on implantable biomaterials was on bioinert materials [87]. However, this approach to replacement of tissues was altered after the implantation of bioactive glasses in the femurs of rats [89–91]. Bioactive glasses have been used as implant materials in the human body to repair and replace diseased or damaged bone. The formation of apatite layer promotes the adhesion of bone tissues to the implant and enhances bone repair or reconstruction [93]. When compared with synthetic hydroxyapatite, bioactive glasses offer superior properties such as gene activation, high level of bioactivity, and a better bone regenerative capability [94]. This section briefly covers the physical and biological properties of bioactive glasses.

Table 4 Composition of bioactive glasses and glass-ceramics used for medical and dental applications. Reprinted from Ref. [87] (Copyright © 2013 Hench, open access under the Creative Commons Attribution License).

Composition (wt%)	45S5 Bioglass (NovaBone)	S53P4 (AbminDent1)	A-W Glass-ceramic (Cerabone)
Na_2O	24.5	23	0
CaO	24.5	20	44.7
CaF_2	0	0	0.5
MgO	0	0	4.6
P_2O_5	6	4	16.2
SiO_2	45	53	34
Phases	Glass	Glass	Apatite beta-wollastonite Glass
Class of bioactivity	A	B	B

3.2 Bioglass® 45S5

3.2.1 Synthesis

Hench and coworkers have highlighted the very different characteristics of some low-silica compositions of melt-derived soda-lime-phosphate-silicate glasses, of which Bioglass® 45S5 is the most representative member [87, 89, 92]. In these studies, the glass composition included 45 wt% SiO_2, network modifiers of 24.5 wt% Na_2O and 24.5 wt% CaO, as well as 6 wt% P_2O_5 in order to simulate the Ca/P constituents of hydroxyapatite (HA) [89]. The presence of Na ions makes it easier to melt, homogenize, and cast the glass. Moreover, Na ions dissolve from the glass and aid in maintaining a physiological balance of sodium while modifying the local pH. The role of SiO_2 is network forming and strongly decreases the solubility rate of the other ions, thus, providing stability to the materials system [89].

The high bioactivity of 45S5 glasses (Table 4) is based on the ability to form a biological apatite layer when immersed in a physiological solution or implanted *in vivo* [89]. The compositions of the key bioactive glasses used in biomedical applications are shown in Figure 9 [95]. Those located in region "A" represent class-A bioactive materials, known for their ability to regenerate and replace tissue. Bioglass® 45S5 lies at the center of the ternary diagram shown in Figure 9 [95]. The dissolution of class-A bioactive glasses leads to the release of specific amounts of Si, P, Na, and Ca ions, which can approach critical values needed to stimulate the cellular activity. The partial

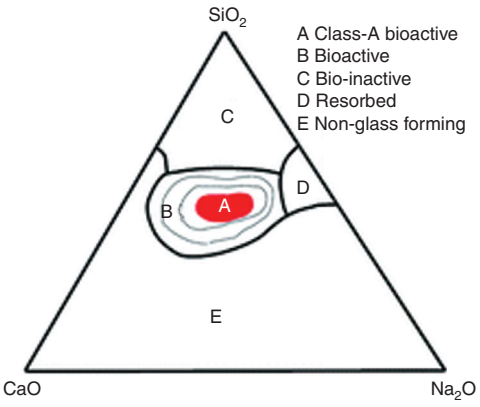

Figure 9 Kinetic diagram of bioactivity [92]. Only compositions inside region B are bioactive and form a bond with bone. Bioactivity inside this region increases going toward the center (region A). Reprinted with permission from Ref. [95]. Copyright © 2010 Royal Society of Chemistry.

dissolution and ion release govern both the apatite deposition and the gene-activation processes [95, 96]. Silicate glasses within region C, such as window glass, behave as nearly inert materials and elicit formation of a fibrous capsule at the interface of implant tissue. Glasses within region D are resorbable and disappear within 10–30 days post-implantation, whereas those within region E are not glass-forming materials, thus, have not been tested as implants [92].

All early bioactive glass processing involved melting the glass at high temperatures followed by casting of bulk implants or quenching of powders [97], which resulted in dense or low porosity texture materials [98]. In melt quenching of Bioglass® 45S5 or other commercial bioactive glasses, oxides are melted together in a platinum crucible at high temperatures (above 1300°C) and quenched either in water (frit) or in a graphite mold (for rods or monoliths) [88]. The original Bioglass® 45S5 was prepared at a melting temperature of 1450°C, homogenization time of 18–24 h, and annealing temperature of 450°C for 1–4 h [89].

In 1991, Li et al. [99] showed that a stable bioactive gel-glass could be made by the sol-gel process. This method makes it possible to produce glasses that cannot be obtained with conventional melting processes [100]. The sol-gel route is essentially a chemistry-based synthesis route that forms and assembles nanoparticles of silica at room temperature [88]. During this process, a solution containing the compositional precursors undergoes polymer-type reactions at room temperature to form a gel [88, 101]. The produced gel is a wet inorganic network of covalently bonded silica, which upon drying and heating (e.g., to 600°C) becomes a glass [88]. The sol-gel process has the potential to enable molecular and textural tailoring of the biological behavior of new bioactive materials [97].

A wide range of shapes and forms, including particles, fibers, foams, porous scaffolds, coatings, and net shape monoliths can be made by the sol-gel process [97]. Mesopores in the nanometer-size range can be achieved as well as macropores in the range of 100–500 μm. Surfaces of the bioactive gel-glasses can be modified by a variety of surface chemistry methods [97]. Moreover, glasses made by the sol-gel process show bioactivity in a larger compositional range than that of melt-derived systems [102]. In addition, the porous microstructure of sol-gel-derived glasses may promote protein absorption and cell adhesion due to the high specific surface area [103].

The sol-gel process can be limiting in terms of composition, high remaining water or solvent content at low process temperatures, and generally requires the use of an annealing or sintering step after preparation [98]. The latter promotes the formation of hard agglomerates of glass nanoparticles. Brunner et al. [98] reported on the preparation of bioactive glass nanopowders using flame synthesis. The goal was to demonstrate that the direct preparation of glass nanoparticles in a high-temperature environment could offer advantages in terms of glass particle size, homogeneity, as well as accessible compositions. The evolution of the pore size distribution during sintering of Bioglass® 45S5 samples measured by mercury intrusion porosimetry is shown in Figure 10. Increasing the sintering temperature led to a pronounced shift in the pore size distribution. As-prepared glass nanopowders exhibited a relatively narrow pore size distribution (20–60 nm), which was attributed to interparticle pores.

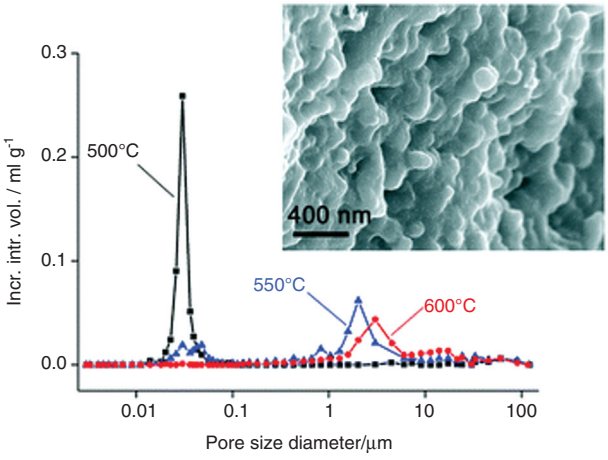

Figure 10 Mercury intrusion porosimetry of calcined Bioglass® 45S5 samples. Inset: Scanning electron micrograph after sintering at 600°C. Reprinted with permission from Ref. [98]. Copyright © 2006 Royal Society of Chemistry.

The sintering started at around 500°C, while the pores partially collapsed at 550°C leading to a bimodal pore size distribution, featuring unaffected pores around 30–60 nm and large pores in the micrometer range. At 600°C, the material mainly consisted of a microporous glass ceramic (inset, Figure 10).

3.2.2 Physical properties

In a review article, Jones [88] has elaborated on the recent developments aimed at improving the properties of bioactive glasses. Some of the current scientific challenges associated with these glasses are due to the limitations of the original Bioglass® 45S5 [88]. Unlike calcium phosphates that are widely used in the clinic, the difficulty in producing porous scaffolds made of bioactive glasses has limited their use in bone regeneration. For example, Bioglass® 45S5 crystallizes during sintering; therefore, the glass composition needs to be tailored to prevent crystallization. Synthesizing sol-gel glasses, where the silica network is assembled at room temperature, can also help to avoid the sintering problems [88]. Sol-gel-derived bioactive glasses with different compositions, such as 70S30C (70 mol% SiO_2, 30 mol% CaO), have shown the ability to produce 3D scaffolds (foams) with interconnected pore morphologies similar to the hierarchical structure of trabecular bone [104].

One of the primary limitations on clinical use of bioceramics, including bioactive glasses, is the uncertain lifetime under the complex physiological loading conditions, slow crack growth, and cyclic fatigue encountered in many clinical applications (Table 5) [92]. One potential solution to overcome these mechanical shortcomings is the use of bioceramics as coatings on implantable biomaterials and medical devices [92, 103]. An alternative approach is to incorporate them as biologically active phases into composite systems. The latter has been briefly covered at the end of this paper. The compositions and mechanical properties of various bioactive glasses

Table 5 Composition and mechanical properties of bioactive ceramics used clinically. Reprinted with permission from Ref. [92]. Copyright © 2005 John Wiley and Sons.

Property	Bioglass 45S5	S45PZ	Glass-ceramic Ceravital	Glass-ceramic Cerabone A/W	Glass-ceramic Ilmaplant Ll	Glass-ceramic Bioverit	Sintered hydroxyapatite $Ca_{10}(PO_4)_6(OH)_2$ (>99.2%)	Sintered β-$3CaO{\cdot}P_2O_5$ (>99.7%)
Composition (wt%)								
Na_2O	24.5	24	5–10	0	4.6	3–8		
K_2O	0		0.5–3.0	0	0.2	3–8		
MgO	0		2.5–5.0	4.6	2.8	2–21		
CaO	24.5	22	30–35	44.7	31.9	10–34		
Al_2O_3	0		0	0	0	8–15		
SiO_2	45.0	45	40–50	34.0	44.3	19–54		
P_2O_5	6.0	7	10–50	16.2	11.2	2–10		
CaF_2	0			0.5	5.0	3–23		
B_2O_3	0	2						
Phase[a]	Glass	Glass	Apatite glass	Apatite β-wollastonite glass	Apatite β-wollastonite glass	Apatite phlogopite glass	Apatite	Whitlockite
Density (g/cm³)	2.6572			3.07		2.8	3.16	3.07
Vickers hardness (HV)	458±9.4			680		500	600	
Compressive strength (MPa)			500	1080		500	500–1000	460–687
Bending strength (MPa)	42[b]			215	160	100–160	115–200	140–154
Young's modulus (GPa)	35		100–150	218		70–88	80–110	33–90
Fracture toughness, K_{IC} (MPa·m$^{1/2}$)				2.0	2.5	0.5–1.0	1.0	
Slow crack growth, *n* (unitless)				33			12–27	

[a]Apatite is $Ca_{10}(PO_4)_6(O,F)$, β-wollastonite is $CaO{\cdot}SiO_2$, phlogopite is $(Na,K)Mg_3(AlSiO_{10})F_2$, and whitlockite is β-$3CaO{\cdot}P_2O_5$. [b]Tensile.

and glass-ceramics are compared in Table 5. It can be seen that the strength and Young's modulus of Bioglass® 45S5 are lower than those of the other bioactive ceramics listed in Table 5 [92].

Bioactive glass scaffolds with compressive strengths comparable to those of trabecular bone have been developed using several fabrication methods; however, these scaffolds have potential for the repair of nonloaded bone defects [105]. By optimizing the composition, sintering conditions, and thermal history, developing bioactive glass scaffolds with strength comparable to human cortical bone seems to be feasible, which could potentially be used for the repair of loaded bone defects [105, 106]. The use of biocompatible polymer coating has been proposed as a method for improving the toughness of bioactive glass scaffolds, which could provide a crack bridging mechanism through energy dissipation by the polymer layer [105]. This is similar to the crack bridging mechanism role reported for collagen fibrils in native bone, which plays an important role in the toughness of bone tissue [107]. Finally, Figure 11 shows a 3D slice through material property space, comparing the Young's modulus, strength, and density of different natural and synthetic materials [108]. These properties can be compared with those of cortical and cancellous bone listed in Table 2.

3.2.3 Biological properties

When melt-processed bioactive glasses are subjected to body fluids, they bond chemically to human tissues by the precipitation of the amorphous calcium phosphate (ACP) layer that later transforms into Ca-deficient nanocrystalline hydroxy-carbonate apatite (HCA) [109]. Hench and coworkers [110, 111] suggested a five-step reaction sequence accounting for the formation of HCA as shown in Figure 12 [109]. The first three steps involve reactions between the silicate surface and the body fluid, followed

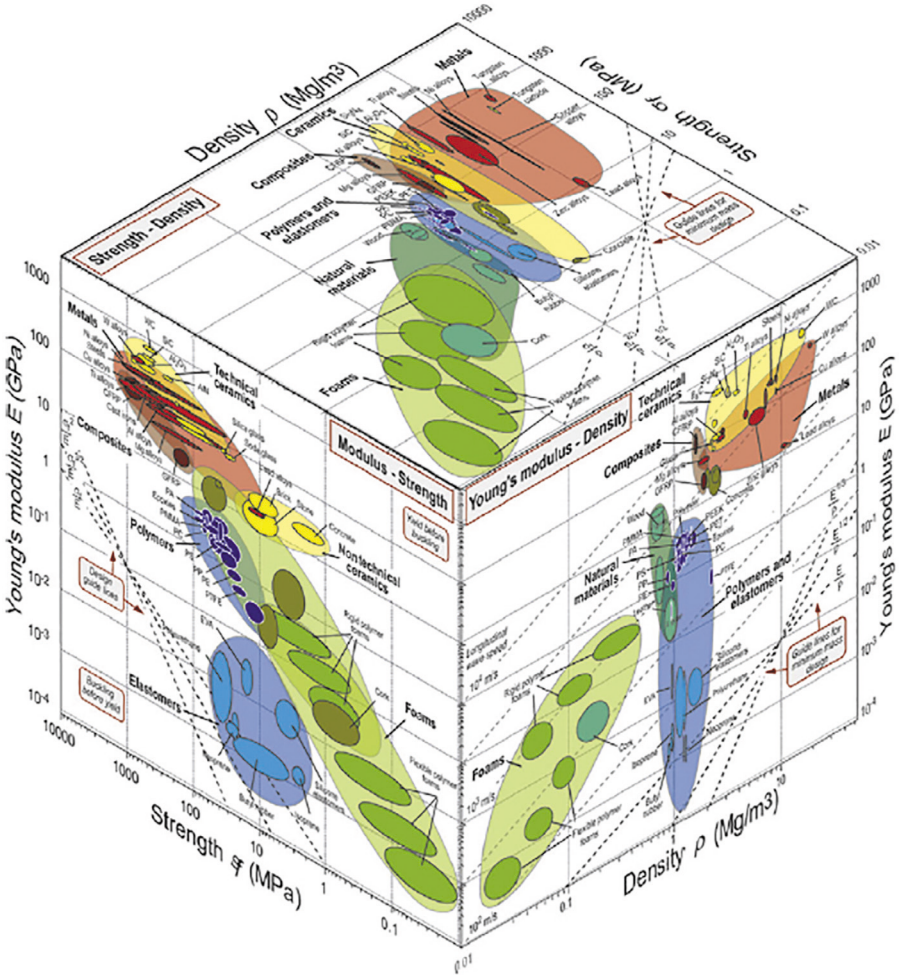

Figure 11 A 3D slice through material property space: the modulus-strength-density slice. Reprinted with permission from Ref. [108]. Copyright © 2011 Michael F. Ashby; published by Elsevier.

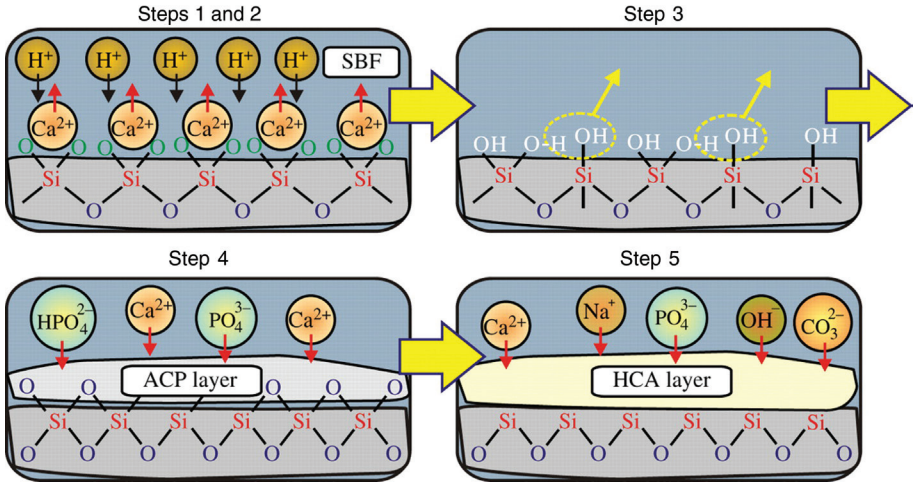

Figure 12 Schematic illustration of the reaction sequence leading to HCA formation according to Hench and coworkers [110, 111], assuming a melt-processed CaO-SiO_2 glass. Reprinted from Ref. [109] (Copyright © 2013 Gunawidjaja et al., open access under the Creative Commons Attribution License).

by the breakage of Si-O-Si bonds leading to the formation of Si-OH groups and repolymerization. Step 4 shows the formation of amorphous calcium phosphate (ACP), followed by crystallization (HCA) in step 5 that involves the uptake of additional ions such as OH- and Na+ [109].

In vivo studies have shown that bioactive glasses bond with bone more rapidly than other bioceramics, and *in vitro* studies indicate that their osteogenic properties are due to their dissolution products stimulating osteoprogenitor cells at the genetic level [88]. Controlled release of biologically active Ca and Si ions from bioactive glasses leads to the upregulation and activation of seven families of genes in osteoprogenitor cells that give rise to rapid bone regeneration. Recent findings also indicate that controlled release of lower concentrations of ionic dissolution products from bioactive glasses can be used to induce angiogenesis and thereby offer potential for design of gene-activating glasses for soft tissue regeneration [112]. In addition, it has been reported that the ionic dissolution products released from Bioglass® 45S5 influence the cell cycle of osteogenic precursor cells and ultimately control the differentiated cell population [113, 114].

In general, it is believed that apatite-forming ability of bioceramics (e.g., Bioglass® 45S5, HA, and glass-ceramic A-W) is primarily due to their composition, which contains HA or its components such as CaO and P_2O_5. However, the assessment of different bioceramics for apatite-forming ability in SBF implies that CaO and P_2O_5 are not the essential components for apatite formation [115]. Figure 13 shows the dependence of apatite formation in SBF to the glass composition. Interestingly, in CaO-P_2O_5-SiO_2 systems, the glass composition that forms an apatite layer

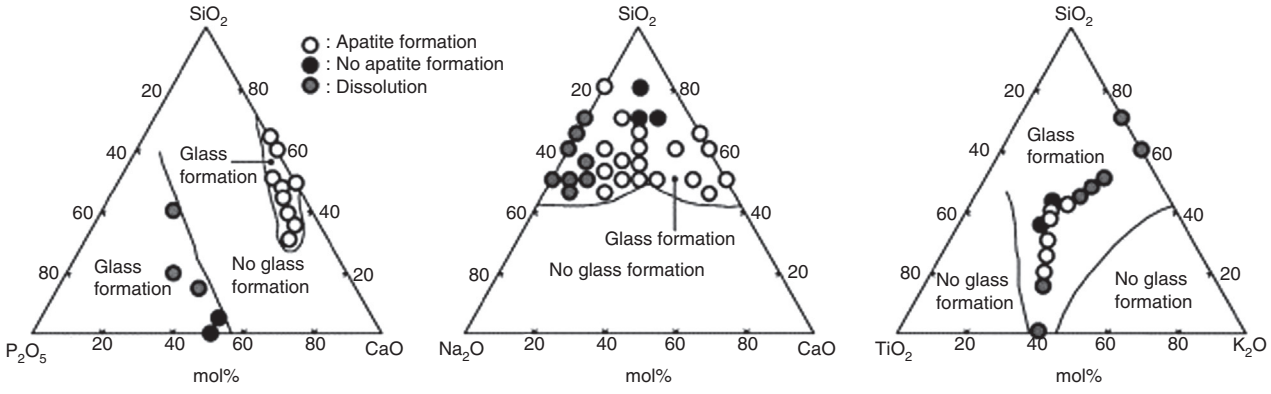

Figure 13 Dependence of apatite formation on glass composition for CaO-P_2O_5-SiO_2, Na_2O-CaO-SiO_2, and K_2O-SiO_2-TiO_2 systems, respectively, after soaking in SBF for 28 days. Reprinted with permission from Ref. [115]. Copyright © 2003 Elsevier.

in SBF is based on the CaO-SiO_2 system (not on the CaO-P_2O_5 system) [115]. This glass composition has also shown to bond to bone *in vivo* by forming apatite on the surface [116]. Based on Figure 13, the CaO- and P2O5-free Na_2O–SiO_2 glasses, as well as K_2O-TiO_2-based glasses, can also form apatite in SBF. The mechanism for apatite formation in these glass systems has been elaborated by Kokubo et al. [115].

Biomaterials based on bioactive glasses exhibit enhanced biocompatibility and bioactivity upon reducing the glass particle size [117]. The increasing specific surface area and pore volume of bioactive glasses may greatly accelerate the deposition of hydroxyapatite (HA) by the biomimetic process [117, 118]. In a recent study, de Oliveira et al. [117] reported a significantly higher *in vitro* osteoblast cytocompatibility behavior for bioactive glass nanoparticles (BGNPs), when compared to similar micron-sized particles. The spherical BGNPs (87±5 nm in size) were prepared using the sol-gel process to obtain an oxide-ternary system with the stoichiometric proportion of 60% SiO_2, 36% CaO, and 4% P_2O_5. The improvement in the overall bioactive behavior of BGNPs was attributed to the enhanced interactions at the cell-nanomaterial interfaces caused by the much higher surface area of the nanoparticles [117]. Moreover, the increased HA nucleation on the nanoparticle surfaces was found to be responsible for the higher cell viability and increased alkaline phosphatase (ALP) activity.

The role of particle size on the bioactivity of bioactive glasses has been reported for micron-sized particles as well. Sepulveda et al. [119] investigated the effects of particle size (5–20 μm, 90–300 μm, and 90–710 μm) and type of dissolution medium on the *in vitro* dissolution behavior of bioactive glasses. Melt-derived 45S5 and sol-gel-derived 58S bioactive glass were used in this study. Both glasses showed a dissolution behavior that was directly correlated to their particle size range. The lower the particle size, the higher the dissolution rate became [119]. Therefore, the change in exposed area (particle size variation) was reported to be an efficient way to control dissolution rates of the silicate network. The effect of particle size variation was more pronounced on the dissolution of 45S5 melt-derived powders, when compared with sol-gel-derived glasses [119]. This was attributed to melt-derived glasses being more susceptible to surface area variations due to their inherent low porosity texture, whereas in sol-gel glasses the dissolution behavior and bioactivity depend more on the mesoporous texture than on their surface area [119]. As for the effect of dissolution media, lower dissolution rates were observed in culture media when compared to the simulated body fluid (SBF) [119].

It is well known that both topographic features and chemistry influence the wettability of surfaces [120]. The specific surface area and pore volume of bioactive glasses have shown to influence their wettability. In a study, mesoporous 45S5 bioactive glass-ceramic coatings exhibited higher wettability than that of 45S5 bioactive glass-ceramic coatings, according to their lower water contact angle [121]. Mesoporous materials have microtexture features of high specific surface area and large pore volume, thereby leading to highly hydrophilic surfaces. Similarly, nano-sized bioactive glasses tend to lead to a lower surface contact angle than micro-sized particles when embedded into polymeric membranes (e.g., chitosan) [120]. Apatite layer formed on the surface of polymer/bioactive glass composites, characterized by the assembly of hydrophilic calcium phosphate crystals, has shown to lower the water contact angle [120].

3.3 Other bioactive glasses

Despite the potential benefits of bioactive glasses over synthetic HA and other calcium phosphates, the original Bioglass® 45S5 is difficult to process into fibers, scaffolds, and coatings, which hinders further commercial success for this class of biomaterials [88]. This section covers some recent studies that have looked into modifying the formulation of bioactive glasses in order to improve their physical properties and processability. The emphasis in this section is placed on modifying the thermal properties of bioactive glasses. The following section briefly covers bioactive glass/polymer and HA/polymer composites used as bone tissue engineering scaffolds.

3.3.1 Zn- and Ti-doped bioactive glasses

Zinc, titanium, copper, silver, magnesium, and strontium ions can be introduced in the amorphous matrix of a bioactive glass [88, 122–126]. They are used to improve different characteristics such as the mechanical properties, chemical reactivity, and biological properties. Zinc is an element that presents a physiological interest in medicine due to its effects on implanted biomaterials. Zinc is an important trace element in the human bones and has shown to improve the biomineralization both *in vitro* and *in vivo* [127]. It also takes part in the production of collagen [128], proteins [129], and enzymatic processes [130].

The structural role of ZnO is unique as it can enter the glass network as both a network former and a network modifier [131]. It has been reported that the concentration

of ZnO nanofillers could significantly affect the thermal properties of polymers due to a catalytic effect [132]. The addition of zinc ions to silicate and borosilicate glasses has also shown to improve their thermal properties [133]. Moreover, the presence of Zn can improve the mechanical properties (e.g., fracture strength) and the glass-forming ability [134], while lowering the fusion temperature [133, 134].

Titanium (Ti) is another biomaterial that has been used in medical devices, such as hip implants and screws and plates for bone fracture repair, due to its desirable mechanical properties [135]. The addition of TiO_2 into glass-forming oxide systems usually contributes to the stabilization of their structure and to the improvement of chemical durability, mechanical properties, and electrical conductivity [136]. The chemical durability of the glasses without TiO_2 is usually poor, but the replacement of Na_2O or P_2O_5 by TiO_2 can results in a pronounced increase in chemical durability of a bioactive glass [137]. In borophosphate glasses, the addition of TiO_2 can lead to a nonlinear increase of glass transition temperature [136]. The same phenomenon has been observed in Na_2O-TiO_2-P_2O_5 ternary system glasses by the addition of TiO_2 (from 0 to 5 mol%) [137].

3.3.2 Physical properties

Wers et al. [138] have reported the properties of bioactive glass 46S6 and Zn-doped 46S6. To prepare bioactive glass 46S6, they used sodium metasilicate (Na_2SiO_3), silicon oxide (SiO_2), calcium metasilicate ($CaSiO_3$), and sodium metaphosphate ($Na_3P_3O_9$) [138]. The thermal process used in this study is shown in Figure 14 [138]. The oxides (46 wt% SiO_2, 24 wt% CaO, 24 wt% Na_2O, and 6 wt% P_2O_5) were placed in platinum crucibles inside an electric furnace. After a temperature rise at a rate of 10°C min^{-1}, the samples were held at 900°C for 1 h to achieve decarbonation. The second temperature rise at a rate of 20°C min^{-1} was followed by an isotherm at 1350°C for 3 h. The samples were cast in preheated brass molds, annealed at 565°C for 4 h near the glass transition temperature of the glass to eliminate the residual stresses and ground to obtain glass powder (40-µm particle size).

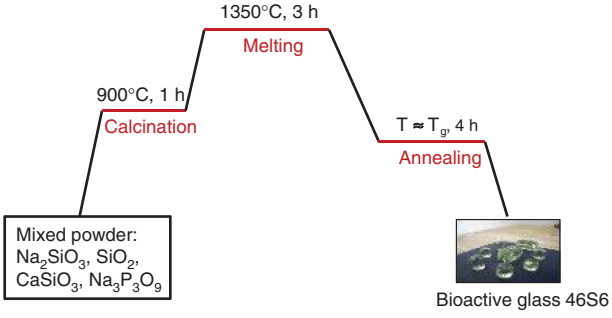

Figure 14 The thermal process for the synthesis of bioactive glass 46S6. Modified from Ref. [138].

Figure 15 shows the effect of zinc content on thermal properties of bioactive glass 46S6. Neither the glass transition temperature (T_g) nor the crystallization temperature (T_c) seems to be affected by the presence of zinc. However, when the amount of zinc increases from 0.1 wt% to 10 wt%, the fusion temperature (T_f) drops from 1219°C to 1109°C. The fusion temperature of the undoped bioactive glass 46S6 is 1230°C.

The effect of Ti on the thermal behavior of 46S6 is presented in Figure 16 [123]. When the Ti content increases from 0.1 wt% to 10 wt%, the crystallization temperature increases from 611°C to 700°C, whereas the effect on the glass transition temperatures is less pronounced (increasing from 548°C to 576°C). The most significant effect caused by the introduction of Ti is the reduction of the fusion temperature (117°C difference between 46S6-0.1Ti and 46S6-10Ti). When the doping metallic oxides are introduced in the amorphous matrix, the covalent Si-O-Si chemical bonds are broken to create metal-oxygen ionic bonds. As covalent bonds are stronger energetically than metal-oxygen ionic bonds, changes in the thermal behavior of glasses are observed [123, 138].

3.3.3 Biological properties

Oudadesse et al. [93] and Wers et al. [122] have investigated the *in vitro* characteristics of 46S6 and Cu-Zn-doped

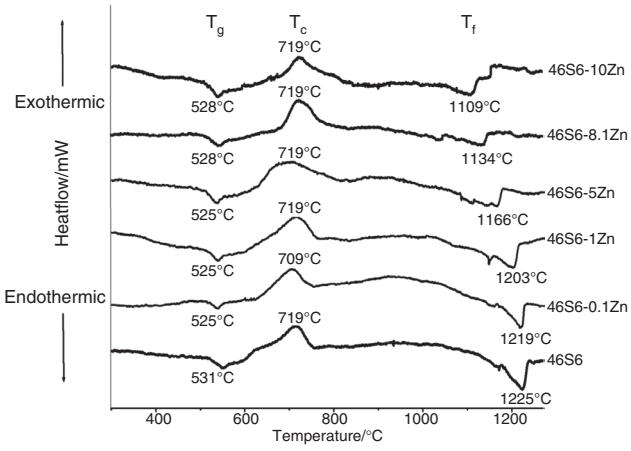

Figure 15 Thermal curves of 46S6 and Zn-doped 46S6. Reprinted with permission from Ref. [139]. Copyright © 2011 Bui and Oudadesse.

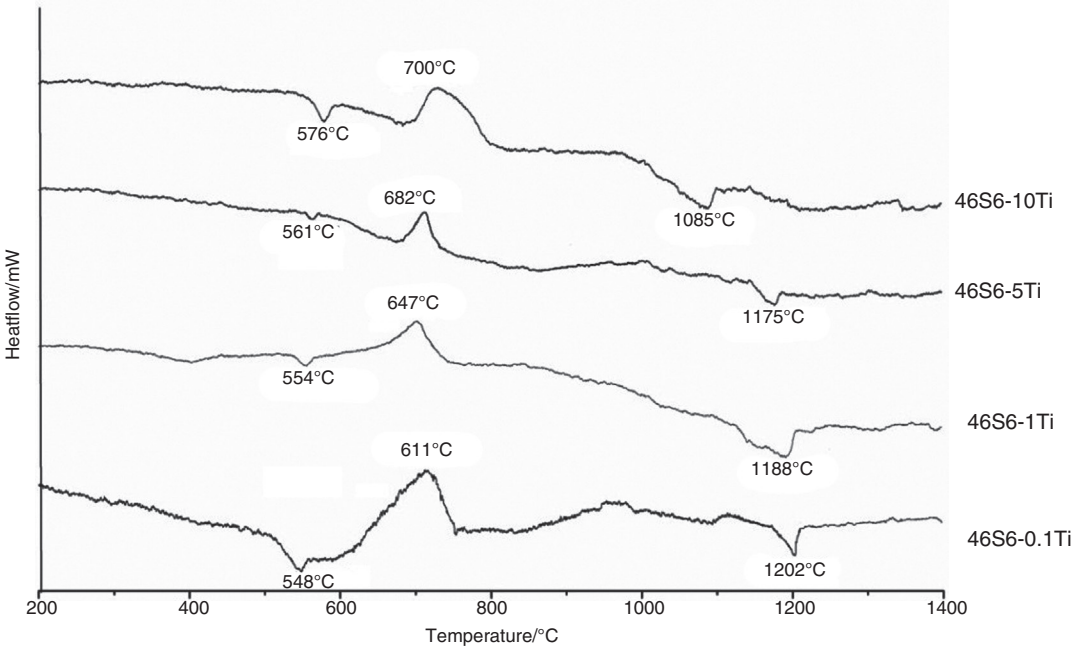

Figure 16 Thermal curves of Ti-doped 46S6 bioactive glasses. Reprinted with permission from Ref. [123]. Copyright © 2014 Elsevier.

46S6 bioactive glasses by soaking the glass powders into the simulated body fluid (SBF) with pH and mineral composition similar to that of human blood plasma. The SBF solution was prepared by dissolving NaCl, $NaHCO_3$, KCl, $K_2HPO_4{\cdot}3H_2O$, $MgCl_2{\cdot}6H_2O$, and $CaCl_2$ in deionized water and buffering with $(CH_2OH)_3CNH_2$ and HCl 6N to obtain a pH value of 7.4 according to Kokubo's technique [140, 141]. The ionic composition of this solution is shown in Table 6. The samples were maintained in SBF at body temperature (37°C) under controlled agitation of 50 rpm for 1, 3, 7, and 30 days. The formation of HA on the glass surface at different time points was confirmed by X-ray diffraction (XRD). The XRD of the initial glass did not show any evidence of crystalline phase, which confirms the amorphous characteristic of the glass. The XRD results after soaking in SBF showed two characteristic peaks of HA at 26° and 32°, where the intensity increased with time and became more pronounced after 30 days. Fourier transform infrared spectroscopy (FTIR) was also used to detect the appearance of HA by the bands at 563 and 606 cm^{-1} [93]. The SEM micrographs taken from the surface of 46S6 showed the presence of a homogeneous and well-crystallized hydroxyapatite (HA) layer after 30 days (Figure 17A) [122]. The apatite layer on the surface of 46S6 doped with 0.1% Cu and 0.1% Zn (Figure 17B) showed almost the same morphology, but the size of crystals was different, and the apatite layer was more heterogeneous. The mixture of Cu and Zn in the glassy matrix appeared to improve cell proliferation.

The presence of other ions in a doped bioactive glass can also affect the biological properties. For example, strontium can be substituted for calcium in a bioactive glass to increase osteoblast proliferation and ALP activity, while inhibiting osteoclast-mediated resorption of CaP films [126]. Therefore, incorporation of strontium into bioactive glasses could be an effective way of delivering a steady supply of strontium ions to a bone defect site in osteoporotic patients [88, 126, 142]. In another study, incorporation of Ag_2O into a bioactive glass enabled antimicrobial properties without compromising its bioactivity [124]. Antibacterial surfaces are of particular interest for reducing biomaterial-centered infection and, thereby, enhancing tissue integration and bone regeneration [124, 143, 144].

Table 6 Ionic composition of the SBF solution, 10^{-3} mol l^{-1} [141].

Ions	Na^+	K^+	Ca^{2+}	Mg^{2+}	Cl^-	HCO_3^-	HPO_4^{2-}
SBF	142.0	5.0	2.5	1.5	147.8	4.2	1.0
Plasma	142.0	5.0	2.5	1.5	103.0	27.0	1.0

4 Bioceramic/polymer composites for bone reconstruction

Composites based on biodegradable polymers and bioceramics (e.g., calcium phosphates and bioactive glasses)

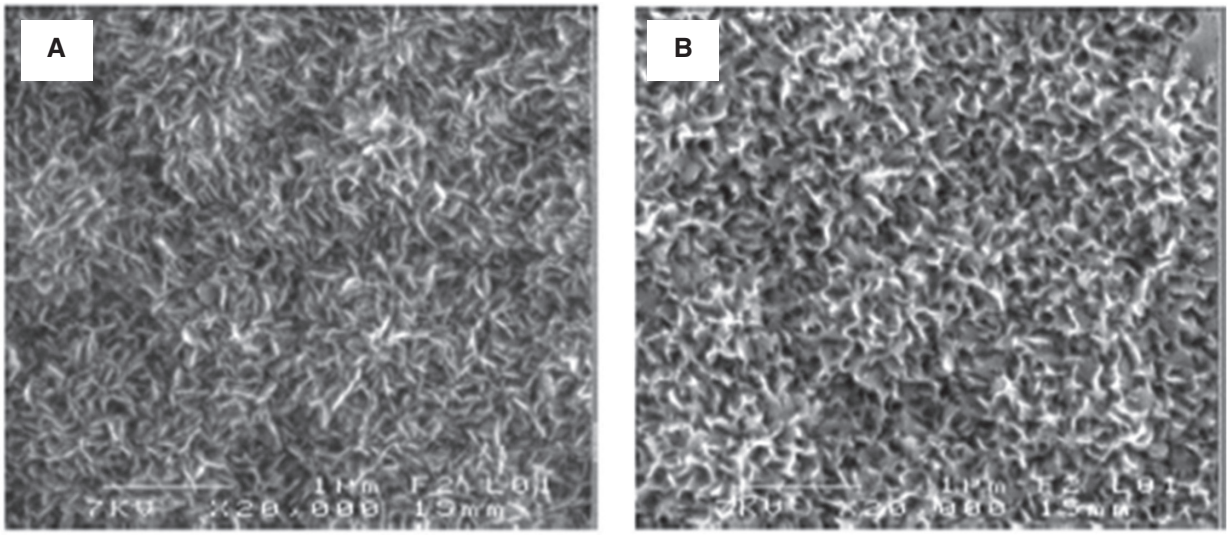

Figure 17 Hydroxyapatite layer on the surface of the (A) 46S6 and (B) 46S6 doped with 0.1% Cu and 0.1% Zn after 30 days of immersion in the SBF. Reprinted from Ref. [122] (Copyright © 2013 Wers et al., open access under the Creative Commons Attribution License).

have attracted much attention in bone reconstruction and repair because of their biological and physicochemical advantages. Polymers used for this purpose include synthetic polymers such as polylactic acid (PLA), polyglycolic acid (PGA), polycaprolactone (PCL), poly(lactic-co-glycolic acid) (PLGA) as well as natural polymers like gelatin, alginate, collagen, chitin, and chitosan [145–153]. Nanocomposite scaffolds consisting of bioactive calcium phosphate nanoparticles and biodegradable polymers have shown promise for bone tissue regeneration [154–156]. Similarly, several biodegradable polymer/bioactive glass composites have shown to possess a good bioactivity and osteoinductivity, as demonstrated by rapid bone repair and the enhancement of bone cell growth and differentiation [157, 158].

Of particular interest is the combination of HA with collagen as a bioactive composite, as this appears to be a natural choice for bone grafting due to the composition of native bone [159]. Such a composite matrix, when seeded with human-like osteoblast cells, has shown better osteoconductive properties compared to monolithic HA and has resulted in calcification of an identical bone matrix [160]. In another study, Vargas et al. [161] investigated the effect of nano-sized Bioglass® 45S5 (n-BG) particles, 20–30 nm in size, on the angiogenic properties of bovine type I collagen/n-BG composites. Two concentrations of n-BG were considered in this study (i.e., 10 wt% and 20 wt%). The addition of a limited concentration (10 wt%) of n-BG to collagen films induced an early angiogenic response, suggesting that this collagen/n-BG composition could be an attractive matrix for tissue engineering applications [161].

Chitosan is another biomaterial that has drawn attention as a polymer matrix for embedding bioactive micro- and nanoparticles. Chitosan is a low-cost natural biodegradable polymer obtained by partial deacetylation of chitin. It is considered as a suitable material for biomedical applications because of its nontoxic character, good biocompatibility, non-antigenicity, antitumor activity, and protein adsorption properties. It promotes cell adhesion and migration, enhances wound healing, and has tunable biodegradation rate by controlling its degree of deacetylation, molecular weight, and crystallinity [162–164]. Chitosan is tough and flexible, but lacks sufficient strength to be used alone in load-bearing applications. On the other hand, bioactive glasses are well known for their use as bone implant materials; however, they are characterized by being brittle. Composites made of these two biomaterials have a good likelihood of providing better mechanical properties while supporting tissue healing.

A combination of wet-spun chitosan fibers with bioactive glasses have shown to enhance the material bioactivity and promote osteoblast proliferation and ALP activity [165]. Composites of chitosan and bioactive glasses can be prepared by a wide range of fabrication techniques. Figure 18A shows a typical process for the synthesis of chitosan/bioactive glass composites [93, 139]. First, a solution of chitosan (CH) in acetic acid is prepared (1 wt%), stirred, and filtered to obtain a homogeneous viscous polymer solution. A bioactive glass (e.g., 46S6) suspension is also prepared by ultrasonication of the glass particles in 2 ml of 1 wt% acetic acid for 30 min. Then, the prepared suspension is introduced into the chitosan solution and

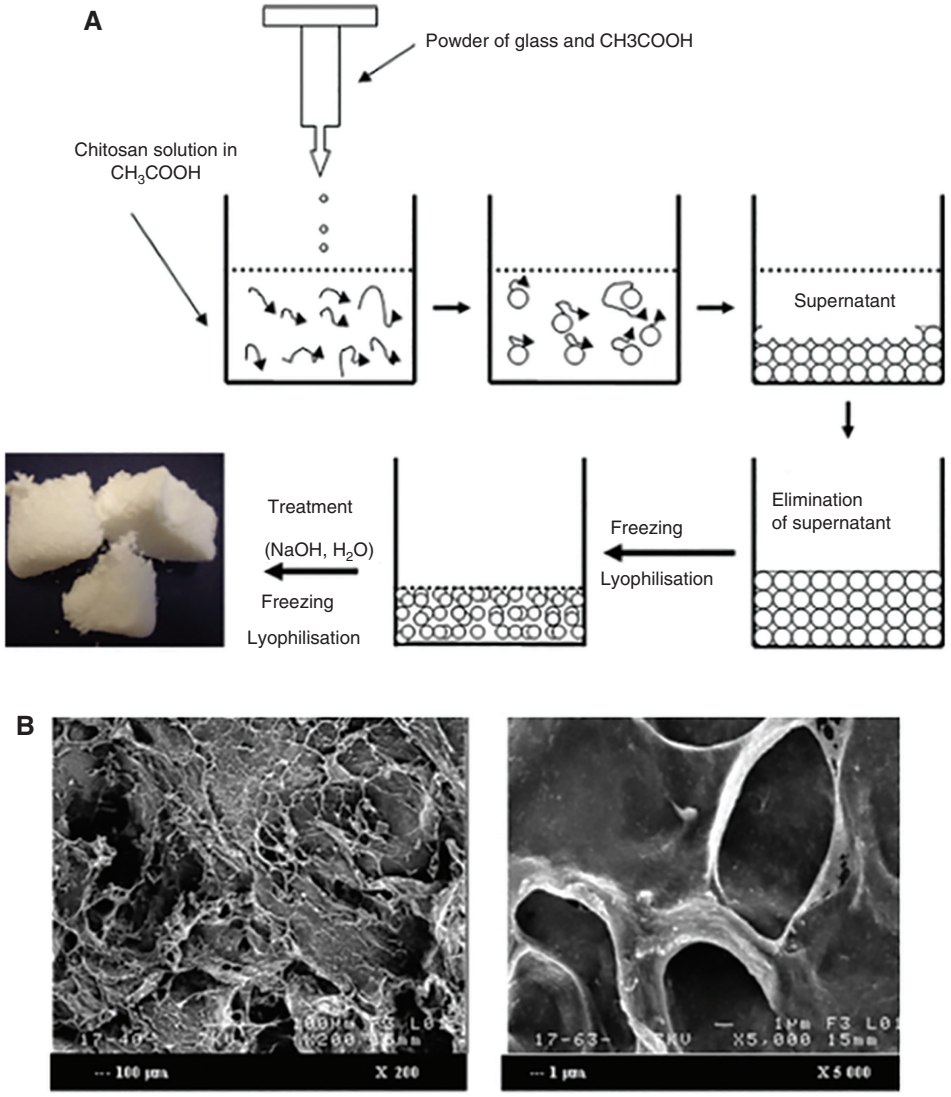

Figure 18 (A) A process for the production of bioactive glass 46S6/chitosan composites; (B) SEM images showing the morphology of the produced composite. Reprinted with permission from Ref. [139]. Copyright © 2011 Bui and Oudadesse.

stirred at 1200 rpm for 2 h to obtain a homogeneous mixture. After eliminating surplus solution, the mixture of 46S6-CH is immersed in 10% NaOH solution for 2 h and washed several times with distilled water to neutralize the residues of acetic acid. Finally, the composites are frozen by liquid nitrogen for 30 min and transferred into a freeze-dryer at -60°C and 1 mbar for 24 h to completely remove the solvent.

The SEM images in Figure 18B show the morphology of the produced composite. The main advantage of the 46S6-CH composite over pure 46S6 is its enhanced bioactivity [139]. The deposition of calcium phosphate allows 46S6-CH to form a chemical bond with the bone tissue. Rapid dissolution of the glassy network in 46S6-CH composite in comparison to 46S6 glass has been observed during *in vitro* experiments [93].

5 Future directions and conclusions

The low tensile strength and brittleness limit the use of calcium phosphates (CaP) and bioactive glasses (BG) in biomedical applications, including bone tissue engineering. It has been reported that a few CaP/polymer composites attain the strength of bone, while most are at the upper limit of porosity compared with cancellous bone [58]. Utilizing inorganic materials with nanoscale features (e.g., submicron grain size) can contribute to the mechanical strength of organic/inorganic composites. However, only few studies provide all of the mechanical characteristics and grain size range used in experiments; which highly limits interpreting and comparing the data [58]. In addition, nano-HA (n-HA) particles, when incorporated into

polymeric scaffolds, have shown to be more osteoconductive than micro-HA particles at the same concentration [166, 167]. Hence, optimization of polymer/n-HA scaffold architecture, composition, and surface topography can help to enhance bone regeneration while improving the mechanical properties.

The mechanical and physicochemical properties of bioactive glasses (BGs) can be tailored by changing the composition, the thermal processing history, and the processing technique [168]. The toughness of BG scaffolds remains a limiting factor for applications in loaded bone repair. The use of a biocompatible polymer coating has been proposed to improve the toughness of bioactive glass scaffolds, which is believed to contribute to energy dissipation by a crack bridging mechanism [105]. The creation of strong and tough bioactive glass scaffolds using advanced fabrication techniques, and their evaluation in loaded bone defect sites in animal models, would pave the way to more extensive use of these materials in bone reconstruction [105].

Nanostructured materials can favor cell adhesion and stimulate new bone growth compared to conventional materials [10]. The nanoscale architecture of adhesion sites plays an important role for the formation of focal adhesions and their dynamics [169]. A progressive restriction of cell spreading has been reported when comparing substrates with decreasing pattern sizes to homogeneous substrates (Figure 19). Therefore, controlling the nanoscale physicochemical properties of the matrix is essential for stem cell expansion and differentiation [169]. In light of this, the role of nanoparticles in altering the surface topography of 3D scaffolds would be an important factor in the success of bone tissue engineering and may require further investigation.

Nano-scale hydroxyapatite (n-HA) functionalized with biomolecules has shown to enhance osteoblast adhesion and bone regeneration [7, 73, 170]. However, the use of nanoparticles also raises the need for a comprehensive understanding of their secondary effect and cytotoxicity in the body [170]. There has been a concern about degradation and wear of biomedical devices that contain nanoscale materials (e.g., with feature sizes <100 nm) as well as needle-shape nanomaterials. Such concerns are largely because the large surface area of nanoparticles makes them very reactive in the cellular environment, while their dimensions enable them to penetrate through the lungs, skin, or intestinal tract causing adverse biological reactions [170]. Hence, investigating the toxicity associated with nanoscale materials is of great importance.

Processing of composite materials is another field that requires further investigation. To date, incorporating substantial amounts of HA particles into electrospun fibers is still a challenge because both micro- and nano-size HA particles tend to agglomerate [56]. The problem of HA particle agglomeration reduces the efficiency of electrospinning, by reducing nanoparticle loading capacity and their poor dispersion within fibrous scaffolds, and thereby leads to mechanically weak scaffolds [56]. Controlling the blending of two dissimilar phases is a critical challenge in the design of inorganic-organic systems [171]. It is anticipated that alternative approaches to the preparation of nanoparticle/polymer composites such as *in situ* precipitation method [64], biomimetic process, and solvent casting [171] could help to resolve the issue of nanoparticle agglomeration while enabling superior mechanical properties than those of conventional composites.

Additive manufacturing (AM) technologies have shown promise in developing scaffolds with rigorously controlled internal architectures and mechanical properties for tissue and organ regeneration [172–174]. However, viscosity constraint is a stumbling block for the majority of extrusion-based AM techniques [175, 176]. Incorporating inorganic nanoparticles poses additional processability challenge due to the increased viscosity, while raising the issue of nonuniform dispersion and agglomeration of nanoparticles. Further advancements in fabrication methods would pave the way to creating organic/inorganic composites and satisfying the load-bearing and bioactivity requirements for bone tissue engineering.

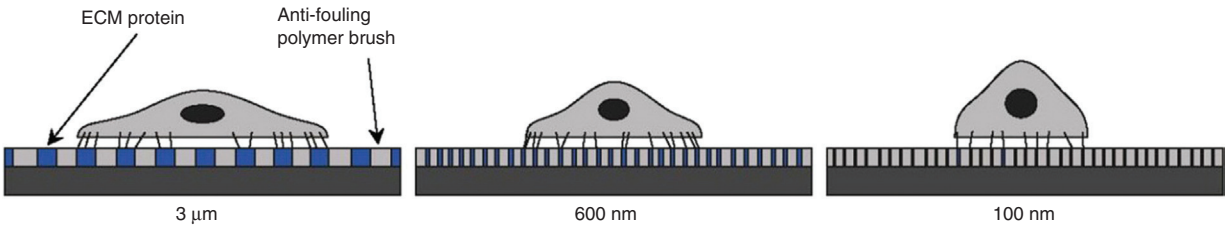

Figure 19 Schematic representation of cells spreading on nanopatterns. Nanoscale geometry of adhesions controls epidermal stem cell spreading and differentiation. Reprinted with permission from Ref. [169]. Copyright © 2014 American Chemical Society.

Finally, in designing tissue-engineered constructs, animal studies are considered to be important in evaluating the surgical feasibility and safety of a medical device. However, efficacy-driven guidelines need to be established from prospective, randomized clinical trials [177]. This is primarily due to the major differences in the biochemical and biomechanical milieu in animal and human joints. Therefore, future studies should look into extending the treatment of degenerative joint pathologies to humans, particularly the aging population [177]. As stem cells appear to possess mechanical memory, which stores information from past physical environments and influences the cell fate [178], culture conditions prior to implantation should be precisely controlled so as to enable meaningful analysis of *in vivo* outcomes.

References

[1] Tran N, Webster TJ. Nanotechnology for bone materials. Wiley Interdiscip. *Rev. Nanomed. Nanobiotechnol.* 2009, 1, 336–351.

[2] Boey FYC, Fuchs H, Chen X. Nanotechnology with soft matter: from structures to functions. *Small* 2011, 7, 1275–1277.

[3] Abidi SSA, Murtaza Q. Synthesis and characterization of nano-hydroxyapatite powder using wet chemical precipitation reaction. *J. Mater. Sci. Technol.* 2014, 30, 307–310.

[4] Porter JR, Ruckh TT, Popat KC. Bone tissue engineering: a review in bone biomimetics and drug delivery strategies. *Biotechnol. Prog.* 2009, 25, 1539–1560.

[5] Schmitz J, Hollinger JO. The critical size defect as an experimental model for craniomandibulofacial nonunions. *Clin. Orthop. Relat. Res.* 1986, 205, 299–308.

[6] Liu Y, Wu G, Groot K De, Liu Y, Wu G, Groot K De. Biomimetic coatings for bone tissue engineering of critical-sized defects. *JR Soc. Interface* 2010, 7, S631–S647.

[7] Li X, Wang L, Fan Y, Feng Q, Cui F-Z, Watari F. Nanostructured scaffolds for bone tissue engineering. *J. Biomed. Mater. Res. A* 2013, 101, 2424–2435.

[8] Lock J, Nguyen TY, Liu H. Nanophase hydroxyapatite and poly(lactide-co-glycolide) composites promote human mesenchymal stem cell adhesion and osteogenic differentiation in vitro. *J. Mater. Sci. Mater. Med.* 2012, 23, 2543–2552.

[9] Taton TA. Nanotechnology: boning up on biology. *Nature* 2001, 412, 491–492.

[10] Zhang L, Webster TJ. Nanotechnology and nanomaterials: promises for improved tissue regeneration. *Nano Today* 2009, 4, 66–80.

[11] Armentano I, Dottori M, Fortunati E, Mattioli S, Kenny JM. Biodegradable polymer matrix nanocomposites for tissue engineering: a review. *Polym. Degrad. Stab.* 2010, 95, 2126–2146.

[12] Bhat SS, Waghmare UV, Ramamurty U. First-principles study of structure, vibrational, and elastic properties of stoichiometric and calcium-deficient hydroxyapatite. *Cryst. Growth Des.* 2014, 14, 3131–3141.

[13] Hench LL, Best SM. Ceramics, glasses, and glass-ceramics: basic principles. In *Biomater. Sci. Introd. Mater. Med.,* 3rd ed., Ratner BD, Hoffman AS, Schoen FJ, Lemons JE, eds., Oxford, UK: Elsevier, 2013, pp. 128–151.

[14] Du L-W, Bian S, Gou B-D, Jiang Y, Huang J, Gao Y-X, Zhao Y-D, Wen W, Zhang T-L, Wang K. Structure of clusters and formation of amorphous calcium phosphate and hydroxyapatite: from the perspective of coordination chemistry. *Cryst. Growth Des.* 2013, 13, 3103–3109.

[15] Dorozhkin SV. Biological and medical significance of nanodimensional and nanocrystalline calcium orthophosphates. In *Biomed. Mater. Diagnostic Devices,* 1st ed., Tiwari A, Ramalingam M, Kobayashi H, Turner APF, Eds., Wiley-Scrivener: Hoboken, NJ, 2012, pp. 19–62.

[16] Zhao X-Y, Zhu Y-J, Lu B-Q, Chen F, Qi C, Zhao J, Wu J. Hydrothermal synthesis of hydroxyapatite nanorods using pyridoxal-5′-phosphate as a phosphorus source. *Mater. Res. Bull.* 2014, 55, 67–70.

[17] Costa DO, Dixon SJ, Rizkalla AS. One- and three-dimensional growth of hydroxyapatite nanowires during sol-gel-hydrothermal synthesis. *ACS Appl. Mater. Interfaces* 2012, 4, 1490–1499.

[18] Kim I-S, Kumta PN. Sol-gel synthesis and characterization of nanostructured hydroxyapatite powder. *Mater. Sci. Eng. B* 2004, 111, 232–236.

[19] Amer W, Abdelouahdi K, Ramananarivo HR, Zahouily M, Fihri A, Djessas K, Zahouily K, Varma RS, Solhy A. Microwave-assisted synthesis of mesoporous nano-hydroxyapatite using surfactant templates. *CrystEngComm* 2014, 16, 543.

[20] Bakan F, Laçin O, Sarac H. A novel low temperature sol–gel synthesis process for thermally stable nano crystalline hydroxyapatite. *Powder Technol.* 2013, 233, 295–302.

[21] Santhosh S, Balasivanandha Prabu S. Thermal stability of nano hydroxyapatite synthesized from sea shells through wet chemical synthesis. *Mater. Lett.* 2013, 97, 121–124.

[22] Tas a C. Synthesis of biomimetic Ca-hydroxyapatite powders at 37 degrees C in synthetic body fluids. *Biomaterials* 2000, 21, 1429–1438.

[23] Hashizume M, Horii H, Kikuchi J, Kamitakahara M, Ohtsuki C, Tanihara M. Effects of surface carboxylic acid groups of cerasomes, morphologically stable vesicles having a silica surface, on biomimetic deposition of hydroxyapatite in body fluid conditions. *J. Mater. Sci. Mater. Med.* 2010, 21, 11–19.

[24] Guo X, Yan H, Zhao S, Li Z, Li Y, Liang X. Effect of calcining temperature on particle size of hydroxyapatite synthesized by solid-state reaction at room temperature. *Adv. Powder. Technol.* 2013, 24, 1034–1038.

[25] Wang X, Qian C, Yu X. Synthesis of nano-hydroxyapatite via microbial method and its characterization. *Appl. Biochem. Biotechnol.* 2014, 173, 1003–1010.

[26] Zakaria SM, Hussein S, Zein S, Othman MR, Yang F, Jansen JA. Nanophase hydroxyapatite as a biomaterial in advanced hard tissue engineering: a review. *Tissue Eng. Part B Rev.* 2013, 19, 431–441.

[27] Kim H, Kim Y, Park S, Rey C, Lee H, Glimcher MJ, Ko JS. Thin film of low-crystalline calcium phosphate apatite formed at low temperature. *Biomaterials* 2000, 21, 1129–1134.

[28] Ge Z, Jin Z, Cao T. Manufacture of degradable polymeric scaffolds for bone regeneration 2008, 3, 022001.

[29] Akbarzadeh R, Yousefi A-M. Effects of processing parameters in thermally induced phase separation technique on porous architecture of scaffolds for bone tissue engineering. *J. Biomed. Mater. Res. Part B Appl. Biomater.* 2014, 102, 1304–1315.

[30] Diggs AB. *Influence of Calcium Phosphate Composition and Design on Bone Regeneration, Degradation and Mechanical Function*. University of Michigan, Ann Arbor, MI, PhD thesis, 2013.
[31] Sun J, Shen Q, Lu J. Comparative study of microstructural remodification to porous β-TCP and HA in rabbits. *Chinese Sci. Bull.* 2009, 54, 2962–2967.
[32] Adams CS, Mansfield K, Perlot RL, Shapiro IM. Matrix regulation of skeletal cell apoptosis. Role of calcium and phosphate ions. *J. Biol. Chem.* 2001, 276, 20316–20322.
[33] Cui Y, Liu Y, Cui Y, Jing X, Zhang P, Chen X. The nanocomposite scaffold of poly(lactide-co-glycolide) and hydroxyapatite surface-grafted with L-lactic acid oligomer for bone repair. *Acta Biomater.* 2009, 5, 2680–2692.
[34] Cai X, Tong H, Shen X, Chen W, Yan J, Hu J. Preparation and characterization of homogeneous chitosan-polylactic acid/hydroxyapatite nanocomposite for bone tissue engineering and evaluation of its mechanical properties. *Acta Biomater.* 2009, 5, 2693–2703.
[35] Ang T, Sultana FS, Hutmacher D, Wong Y, Fuh JY, Mo X, Loh HT, Burdet E, Teoh SH. Fabrication of 3D chitosan–hydroxyapatite scaffolds using a robotic dispensing system. *Mater. Sci. Eng. C* 2002, 20, 35–42.
[36] Wong KL, Wong CT, Liu WC, Pan HB, Fong MK, Lam WM, Cheung WL, Tang WM, Chiu KY, Luk KD, Lu WW. Mechanical properties and in vitro response of strontium-containing hydroxyapatite/polyetheretherketone composites. *Biomaterials* 2009, 30, 3810–3817.
[37] Converse GL, Conrad TL, Roeder RK. Mechanical properties of hydroxyapatite whisker reinforced polyetherketoneketone composite scaffolds. *J. Mech. Behav. Biomed. Mater.* 2009, 2, 627–635.
[38] Gleeson JP, Brien FJO. Composite Scaffolds for Orthopaedic Regenerative Medicine. In *Advances in Composite Materials for Medicine and Nanotechnology*. Attaf B, ed. ISBN: 978-953-307-235-7, InTech, Available from: http://www.intechopen.com.
[39] Ma PX, Zhang R, Xiao G, Franceschi R. Engineering new bone tissue in vitro on highly porous poly(alpha-hydroxyl acids)/hydroxyapatite composite scaffolds. *J. Biomed. Mater. Res.* 2001, 54, 284–293.
[40] Ko HCH, Milthorpe BK, McFarland CD. Engineering thick tissues – the vascularisation problem. *Eur. Cell. Mater.* 2007, 14, 1 – 18; discussion 18–9.
[41] Habraken WJEM, Wolke JGC, Jansen JA. Ceramic composites as matrices and scaffolds for drug delivery in tissue engineering. *Adv. Drug Deliv. Rev.* 2007, 59, 234–248.
[42] Van der Sanden B, Dhobb M, Berger F, Wion D. Optimizing stem cell culture. *J. Cell. Biochem.* 2010, 111, 801–807.
[43] Mendonça G, Mendonça DBS, Aragão FJL, Cooper LF. Advancing dental implant surface technology – from micron- to nanotopography. *Biomaterials* 2008, 29, 3822–3835.
[44] Laurencin CT, Kumbar SG, Prasad S. Nanotechnology and orthopedics: a personal perspective. *Wiley Interdiscip. Rev. Nanomed. Nanobiotechnol.* 2009, 1, 6–10.
[45] Schrader ME. Young-Dupre revisited. *Langmuir* 1995, 11, 3585–3589.
[46] Berg JM, Eriksson LGT, Claesson PM, Borve KGN. Three-component Langmuir-Blodgett films with a controllable degree of polarity. *Langmuir* 1994, 10, 1225–1234.
[47] Vogler EA. Structure and reactivity of water at biomaterial surfaces. *Adv. Colloid Interface Sci.* 1998, 74, 69–117.
[48] Moradi S, Kamal S, Englezos P, Hatzikiriakos SG. Femtosecond laser irradiation of metallic surfaces: effects of laser parameters on superhydrophobicity. *Nanotechnology* 2013, 24, 415302 (12pp).
[49] Rajzer I. Fabrication of bioactive polycaprolactone / hydroxyapatite scaffolds with final bilayer nano-/micro-fibrous structures for tissue engineering application. *J. Mater. Sci.* 2014, 49, 5799–5807.
[50] Ngiam M, Liao S, Patil AJ, Cheng Z, Chan CK, Ramakrishna S. The fabrication of nano-hydroxyapatite on PLGA and PLGA/collagen nanofibrous composite scaffolds and their effects in osteoblastic behavior for bone tissue engineering. *Bone* 2009, 45, 4–16.
[51] Fu S, Wang X, Guo G, Shi S, Liang H, Luo F, YuQuan W, ZhiYong Q. Preparation and characterization of nano-hydroxyapatite/poly (ε-caprolactone)-poly (ethylene glycol)-poly (ε-caprolactone) composite fibers for tissue engineering. *J. Phys. Chem. C* 2010, 114, 18372–18378.
[52] Yang L, Webster TJ. Degradation of implant materials. In *Degrad. Implant Mater.* Eliaz N, ed. New York, NY: Springer New York, 2012, pp. 481–508.
[53] McMahon RE, Wang L, Skoracki R, Mathur AB. Development of nanomaterials for bone repair and regeneration. *J. Biomed. Mater. Res. B Appl. Biomater.* 2013, 101, 387–397.
[54] Liu H, Webster TJ. Nanomedicine for implants: a review of studies and necessary experimental tools. *Biomaterials* 2007, 28, 354–369.
[55] Laschke MW, Strohe a, Menger MD, Alini M, Eglin D. In vitro and in vivo evaluation of a novel nanosize hydroxyapatite particles/poly(ester-urethane) composite scaffold for bone tissue engineering. *Acta Biomater.* 2010, 6, 2020–2027.
[56] Tong H-W, Wang M, Li Z-Y, Lu WW. Electrospinning, characterization and in vitro biological evaluation of nanocomposite fibers containing carbonated hydroxyapatite nanoparticles. *Biomed. Mater.* 2010, 5, 054111.
[57] Jose MV, Thomas V, Johnson KT, Dean DR, Nyairo E. Aligned PLGA/HA nanofibrous nanocomposite scaffolds for bone tissue engineering. *Acta Biomater.* 2009, 5, 305–315.
[58] Wagoner Johnson AJ, Herschler BA. A review of the mechanical behavior of CaP and CaP/polymer composites for applications in bone replacement and repair. *Acta Biomater.* 2011, 7, 16–30.
[59] Eddy G, Poinern J, Brundavanam RK, Fawcett D. Nanometre scale hydroxyapatite ceramics for bone tissue engineering. *Am. J. Biomed. Eng.* 2013, 3, 148–168.
[60] Cunniffe GM, Dickson GR, Partap S, Stanton KT, O'Brien FJ. Development and characterisation of a collagen nano-hydroxyapatite composite scaffold for bone tissue engineering. *J. Mater. Sci. Mater. Med.* 2010, 21, 2293–2298.
[61] Al-Munajjed AA, O'Brien FJ. Influence of a novel calcium-phosphate coating on the mechanical properties of highly porous collagen scaffolds for bone repair. *J. Mech. Behav. Biomed. Mater.* 2009, 2, 138–146.
[62] Liu H, Webster TJ. Mechanical properties of dispersed ceramic nanoparticles in polymer composites for orthopedic applications. *Int. J. Nanomed.* 2010, 5, 299–313.
[63] Roohani-Esfahani S-I, Nouri-Khorasani S, Lu Z, Appleyard R, Zreiqat H. The influence hydroxyapatite nanoparticle shape and size on the properties of biphasic calcium phosphate scaffolds coated with hydroxyapatite-PCL composites. *Biomaterials* 2010, 31, 5498–5509.

[64] Zhang CY, Lu H, Zhuang Z, Wang XP, Fang QF. Nano-hydroxyapatite/poly(L-lactic acid) composite synthesized by a modified in situ precipitation: preparation and properties. *J. Mater. Sci. Mater. Med.* 2010, 21, 3077–3083.
[65] Gay S, Arostegui S, Lemaitre J. Preparation and characterization of dense nanohydroxyapatite/PLLA composites. *Mater. Sci. Eng. C* 2009, 29, 172–177.
[66] Ignjatovic N, Delijic K, Vukcevic M, Uskokovic D. Microstructure and mechanical properties of hot-pressed hydroxyapatite/poly-L-lactide biomaterials. *Bioceramics* 2000, 192, 737–740.
[67] Shikinami Y, Okuno M. Bioresorbable devices made of forged composites of hydroxyapatite (HA) particles and poly-L-lactide (PLLA): Part I. Basic characteristics. *Biomaterials* 1999, 20, 859–877.
[68] Wang H, Zuo YI, Zou QIN, Cheng LIN, Huang DI, Wang LI, Li Y. Nano-hydroxyapatite/polyamide66 composite tissue-engineering scaffolds with anisotropy in morphology and mechanical behaviors. *J. Polym. Sci. Polym. Chem.* 2009, 47, 658–669.
[69] Kim IY, Sugino A, Kikuta K, Ohtsuki C, Cho SB. Bioactive composites consisting of PEEK and calcium silicate powders. *J. Biomater. Appl.* 2009, 24, 105–118.
[70] Okamoto M, John B. Synthetic biopolymer nanocomposites for tissue engineering scaffolds. *Prog. Polym. Sci.* 2013, 38, 1487–1503.
[71] Kim H-W, Knowles JC, Kim H-E. Hydroxyapatite/poly(ε-caprolactone) composite coatings on hydroxyapatite porous bone scaffold for drug delivery. *Biomaterials* 2004, 25, 1279–1287.
[72] Bikiaris DN. Nanocomposites of aliphatic polyesters: an overview of the effect of different nanofillers on enzymatic hydrolysis and biodegradation of polyesters. *Polym. Degrad. Stab.* 2013, 98, 1908–1928.
[73] Webster TJ, Ergun C, Doremus RH, Siegel RW, Bizios R. Specific proteins mediate enhanced osteoblast adhesion on nanophase ceramics. *J. Biomed. Mater. Res.* 2000, 51, 475–483.
[74] Zhou H, Lee J. Nanoscale hydroxyapatite particles for bone tissue engineering. *Acta Biomater.* 2011, 7, 2769–2781.
[75] Cai Y, Liu Y, Yan W, Hu Q, Tao J, Zhang M, Shic S, Tang R. Role of hydroxyapatite nanoparticle size in bone cell proliferation. *J. Mater. Chem.* 2007, 17, 3780.
[76] Aksakal B, Kom M, Tosun HB, Demirel M. Influence of micro- and nano-hydroxyapatite coatings on the osteointegration of metallic (Ti6Al4°V) and bioabsorbable interference screws: an in vivo study. *Eur. J. Orthop. Surg. Traumatol.* 2013, 25, 813–819.
[77] Laquerriere P, Grandjean-Laquerriere A, Addadi-Rebbah S, Jallot E, Laurent-Maquin D, Frayssinet P, Guenounou M. MMP-2, MMP-9 and their inhibitors TIMP-2 and TIMP-1 production by human monocytes in vitro in the presence of different forms of hydroxyapatite particles. *Biomaterials* 2004, 25, 2515–2524.
[78] Grandjean-Laquerriere A, Laquerriere P, Guenounou M, Laurent-Maquin D, Phillips TM. Importance of the surface area ratio on cytokines production by human monocytes in vitro induced by various hydroxyapatite particles. *Biomaterials* 2005, 26, 2361–2369.
[79] Zhao X, Ng S, Heng BC, Guo J, Ma L, Tan TTY, Ng KW, Loo SC. Cytotoxicity of hydroxyapatite nanoparticles is shape and cell dependent. *Arch. Toxicol.* 2013, 87, 1037–1052.
[80] Xu Z, Liu C, Wei J, Sun J. Effects of four types of hydroxyapatite nanoparticles with different nanocrystal morphologies and sizes on apoptosis in rat osteoblasts. *J. Appl. Toxicol.* 2012, 32, 429–435.
[81] Glas SH. *Natur, Struktur und Eigenschaften*. Dritte Neubearbeitete Auflage 1977.
[82] Barton J, Guillemet C. *Le verre: Science et Technologie*. Les Ulis: EDP Sciences, 2004.
[83] Sułowska J, Wacławska I, Szumera M. Effect of copper addition on glass transition of silicate–phosphate glasses. *J. Therm. Anal. Calorim.* 2012, 109, 705–710.
[84] Champagnon M. Influence des effets thermiques et mécaniques sur la relaxation structurale des préformes et des fibres optiques à base de silice Etude par diffusion de la lumière et par diffusion des rayons X. Universit Claude Bernard-Lyon, 2004.
[85] Patel AT, Pratap A. Study of kinetics of glass transition of metallic glasses. *J. Therm. Anal. Calorim.* 2012, 110, 567–571.
[86] Szumera M, Wacławska I. Effect of molybdenum addition on the thermal properties of silicate–phosphate glasses. *J. Therm. Anal. Calorim.* 2012, 109, 649–655.
[87] Hench LL. Chronology of bioactive glass development and clinical applications. *New J. Glass Ceram.* 2013, 3, 67–73.
[88] Jones JR. Review of bioactive glass: from Hench to hybrids. *Acta Biomater.* 2013, 9, 4457–4486.
[89] Hench L, Splinter R, Allen W, Greenlee T. Bonding mechanisms at the interface of ceramic prosthetic materials. *J. Biomed. Mater. Res. Part A* 1971, 5, 117–141.
[90] Beckham C, Greenlee Jr T, Crebo Jr. A. Bone formation at a ceramic implant interface. *Calcif. Tissue Res.* 1971, 8, 165–171.
[91] Greenlee Jr. TK, Beckham CA, Crebo AR, Malmborg JC. Glass ceramic bone implants. *J. Biomed. Mater. Res.* 1972, 6, 235–244.
[92] Hench L. Bioceramics. *Am. Ceram. Soc.* 1998, 81, 1705.
[93] Oudadesse H, Wers E, Bui XV, Roiland C, Bureau B, Akhiyat I, Mostaf A, Chaair H, Benhayoune H, Fauré J. Chitosan effects on glass matrices evaluated by biomaterial. MAS-NMR and biological investigations. *Korean J. Chem. Eng.* 2013, 30, 1775–1783.
[94] Krishnan V, Lakshm T. Bioglass: a novel biocompatible innovation Introduction. *J. Adv. Pharm. Technol. Res.* 2014, 4, 78–83.
[95] Tilocca A. Models of structure, dynamics and reactivity of bioglasses: a review. *J. Mater. Chem.* 2010, 20, 6848.
[96] Hench LL, Polak JM. Third-generation biomedical materials. *Science* (80-) 2002, 295, 1014–1017.
[97] Hench LL. The story of bioglass. *J. Mater. Sci. Mater. Med.* 2006, 17, 967–978.
[98] Brunner TJ, Grass RN, Stark WJ. Glass and bioglass nanopowders by flame synthesis. *Chem. Commun. (Camb)* 2006, 1384–1386. DOI: 10.1039/B517501A.
[99] Li R, Clark AE, Hench LL. An investigation of bioactive glass powders by sol gel processing. *J. Appl. Biomater.* 1991, 2, 231–239.
[100] Klein LC. Chapter 1: Principles, developments, and applications. In *Sol–Gel Technology for Thin Films, Fibres, Preforms, Electronics and Specialty Shapes*, Noyes Publications: Park Ridge, NJ, 1988.
[101] Hench L, West J. The sol–gel process. *Chem. Rev.* 1990, 90, 33–72.
[102] Gallardo J, Galliano P, Duran A. Bioactive and protective sol–gel coatings on metals for orthopaedic prostheses. *J. Sol–Gel Sci. Technol.* 2001, 21, 65–74.

[103] Sola a, Bellucci D, Cannillo V, Cattini A. Bioactive glass coatings: a review. *Surf. Eng.* 2011, 27, 560–572.
[104] Jones JR, Ehrenfried LM, Hench LL. Optimising bioactive glass scaffolds for bone tissue engineering. *Biomaterials* 2006, 27, 964–973.
[105] Fu Q, Saiz E, Rahaman MN, Tomsia AP. Bioactive glass scaffolds for bone tissue engineering: state of the art and future perspectives. *Mater. Sci. Eng. C Mater. Biol. Appl.* 2011, 31, 1245–1256.
[106] Tomsia AP, Division MS, Berkeley L. Bioinspired strong and highly porous glass scaffolds. *Adv. Funct. Mater.* 2012, 21, 1058–1063.
[107] Nalla RK, Kinney JH, Ritchie RO. Mechanistic fracture criteria for the failure of human cortical bone. *Nat. Mater.* 2003, 2, 164–168.
[108] Ashby MF. *Material Property Charts. Mater. Sel. Mech. Des.*, Fourth ed., Oxford, UK: Elsevier Ltd., 2011, p. 57. DOI: 10.1016/B978-1-85617-663-7.00004-7.
[109] Gunawidjaja PN, Mathew R, Andy AYH. Local structures of mesoporous bioactive glasses and their surface alterations in vitro: inferences from solid-state nuclear magnetic resonance. *R. Soc. Publ.* 2012, 370, 1376–1399.
[110] Hench LL. Bioceramics: from concept to clinic. *J. Am. Ceram. Soc.* 1991, 74, 1487–1510.
[111] Clark AE, Pantano CG, Hench LL. Auger spectroscopic analysis of bioglass corrosion films. *J. Am. Ceram. Soc.* 1976, 59, 37–39.
[112] Hench LL. Genetic design of bioactive glass. *J. Eur. Ceram. Soc.* 2009, 29, 1257–1265.
[113] Xynos ID, Hukkanen MVJ, Batten JJ, Buttery LD, Hench LL, Polak JM. Bioglass® 45S5 stimulates osteoblast turnover and enhances bone formation in vitro: implications and applications for bone tissue engineering. *Calcif. Tiss. Int.* 2000, 67, 321–329.
[114] Hench LL, Polak JM, Xynos ID, Buttery LDK. Bioactive materials to control cell cycle. *Mater. Res. Innov.* 2000, 3, 313–323.
[115] Kokubo T, Kim H-M, Kawashita M. Novel bioactive materials with different mechanical properties. *Biomaterials* 2003, 24, 2161–2175.
[116] Ohura K, Yamamuro T, Nakamura T, Kokubo T, Ebisawa Y, Kotoura Y, Oka M. Bone-bonding ability of P2O5-free CaO·SiO2 glasses. *J. Biomed. Mater. Res.* 1991, 25, 357–365.
[117] De Oliveira AAR, de Souza DA, Dias LLS, de Carvalho SM, Mansur HS, de Magalhães Pereira M. Synthesis, characterization and cytocompatibility of spherical bioactive glass nanoparticles for potential hard tissue engineering applications. *Biomed. Mater.* 2013, 8, 025011.
[118] Ostomel T a, Shi Q, Tsung C-K, Liang H, Stucky GD. Spherical bioactive glass with enhanced rates of hydroxyapatite deposition and hemostatic activity. *Small* 2006, 2, 1261–1265.
[119] Sepulveda P, Jones JR, Hench LL. In vitro dissolution of melt-derived 45S5 and sol-gel derived 58S bioactive glasses. *J. Biomed. Mater. Res.* 2002, 61, 301–311.
[120] Caridade SG, Merino EG, Alves NM, Bermudez VDZ, Boccaccini AR, Mano JF. Chitosan membranes containing micro or nano-size bioactive glass particles: evolution of biomineralization followed by in situ dynamic mechanical analysis. *J. Mech. Behav. Biomed. Mater.* 2013, 20, 173–183.
[121] Huang K, Cai S, Xu G, Ye X, Dou Y, Ren M, Wang X. Preparation and characterization of mesoporous 45S5 bioactive glass–ceramic coatings on magnesium alloy for corrosion protection. *J. Alloys Compd.* 2013, 580, 290–297.
[122] Wers E, Bunetel L, Oudadesse H, Lefeuvre B, Mostafa A, Pellen P. Effect of copper and zinc on the bioactivity and cells viability of bioactive glasses. Bioceram. Dev. Appl. 2013, S1, 1–3.
[123] Wers E, Oudadesse H, Lefeuvre B, Bureau B, Merdrignac-Conanec O. Thermal investigations of Ti and Ag-doped bioactive glasses. *Thermochim. Acta* 2014, 580, 79–84.
[124] Bellantone M, Coleman NJ, Hench LL. Bacteriostatic action of a novel four-component bioactive glass. *J. Biomed. Mater. Res.* 2000, 51, 484–490.
[125] Jebahi S, Oudadesse H, Abdessalem N, Keskes H, Rebai T, el Feki H, el Feki A. Comparative study of bone microarchitectural structure after porous bioglass and strontium doped bioactive glass bone graft in Wistar rat model. 2014, 3, 16–20.
[126] Gentleman E, Fredholm YC, Jell G, Lotfibakhshaiesh N, O'Donnell MD, Hill RG, Stevens MM. The effects of strontium-substituted bioactive glasses on osteoblasts and osteoclasts in vitro. *Biomaterials* 2010, 31, 3949–3956.
[127] Storrie H, Stupp SI. Cellular response to zinc-containing organoapatite: an in vitro study of proliferation, alkaline phosphatase activity and biomineralization. *Biomaterials* 2005, 26, 5492–5499.
[128] Wu X, Itoh N, Taniguchi T, Nakanishi T, Tatsu Y, Yumoto N, Tanaka K. Zinc-induced sodium-dependent vitamin C transporter 2 expression: potent roles in osteoblast differentiation. *Arch. Biochem. Biophys.* 2003, 420, 114–120.
[129] Sauer GR, Wuthier RE. Influence of trace metal ions on matrix vesicle calcification. *Bone Miner.* 1992, 17, 284–289.
[130] Sauer GR, Wu LN, Iijima M, Wuthier RE. The influence of trace elements on calcium phosphate formation by matrix vesicles. *J. Inorg. Biochem.* 1997, 65, 57–65.
[131] Veres R, Vanea E, Gruian C, Baia L, Simon V. The effects of PEG assisted synthesis and zinc addition on gamma irradiated bioactive glasses. *Compos. Part B Eng.* 2014, 66, 83–88.
[132] Gaur MS, Singh PK, Chauhan RS. Structural and thermal properties of polysulfone-ZnO nanocomposites. *J. Therm. Anal. Calorim.* 2012, 111, 743–751.
[133] Gao P, Xue Z, Liu G, Zhang J, Zhang M. Effects of Zn on the glass forming ability and mechanical properties of MgLi-based bulk metallic glasses. *J. Non Cryst. Solids* 2012, 358, 8–13.
[134] Karbasi M, Saidi A, Aryanpour G. Study of structure and usage of mechanically alloyed nanocrystalline Ti–Cu–Zn powders in powder metallurgy. *Powder Metall.* 2008, 51, 250–253.
[135] Niinomi M. Mechanical properties of biomedical titanium alloys. *Mater. Sci. Eng. A* 1998, 243, 231–236.
[136] Pospíšil J, Mošner P, Koudelka L. Thermal behaviour and crystallization of titanium–zinc borophosphate glasses. *J. Therm. Anal. Calorim.* 2006, 84, 479–482.
[137] Mošner P, Vosejpková K, Koudelka L. Thermal behaviour and properties of Na2O-TiO2-P2O5 glasses. *J. Therm. Anal. Calorim.* 2009, 96, 469–474.
[138] Wers E, Oudadesse H. Thermal behaviour and excess entropy of bioactive glasses and Zn-doped glasses. *J. Therm. Anal. Calorim.* 2013, 115, 2137–2144.
[139] Bui XV. Élaboration de biomatériaux verres-substances actives (zolédronate-chitosane): caractérisations physico-chimiques: expérimentations "in vitro." University of Rennes 1, France, 2011.

[140] Kokubo T, Kushitani H, Sakka S, Kitsugi T, Yamamuro T. Solutions able to reproduce in vivo surface-structure changes in bioactive glass-ceramic A-W. *J. Biomed. Mater. Res.* 1990, 24, 721–724.
[141] Dietrich E, Oudadesse H, Lucas-Girot A, Mami M. In vitro bioactivity of melt-derived glass 46S6 doped with magnesium. *J. Biomed. Mater. Res. A* 2009, 88, 1087–1096.
[142] Bonnelye E, Chabadel A, Saltel F, Jurdic P. Dual effect of strontium ranelate: stimulation of osteoblast differentiation and inhibition of osteoclast formation and resorption in vitro. *Bone* 2008, 42, 129–138.
[143] Goh Y, Alshemary AZ, Akram M, Rafiq M, Kadir A. Bioactive glass: an in-vitro comparative study of doping with nanoscale copper and silver particles. Int. J. Appl. Glass Sci. 2014, DOI: 10.1111/ijag.12061.
[144] Vulpoi A, Simon V, Ylanen H, Simon S. Development and in vitro assessment of bioactive glass/polymer nanostructured composites with silver. *J. Compos. Mater.* 2012, 48, 63–70.
[145] Rich J, Jaakkola T, Tirri T, Närhi T, Yli-Urpo A, Seppälä J. In vitro evaluation of poly(epsilon-caprolactone-co-DL-lactide)/ bioactive glass composites. *Biomaterials* 2002, 23, 2143–2150.
[146] Walsh D, Furuzono T, Tanaka J. Preparation of porous composite implant materials by in situ polymerization of porous apatite containing epsilon-caprolactone or methyl methacrylate. *Biomaterials* 2001, 22, 1205–1212.
[147] Devin JE, Attawia MA, Laurencin CT, Moorehead-laurencin HI. Three-dimensional degradable porous polymer-ceramic matrices for use in bone repair. *J. Biomater. Sci. Polym.* 1996, 7, 661–669.
[148] Leonor IB, Baran ET, Kawashita M, Reis RL, Kokubo T, Nakamura T. Growth of a bonelike apatite on chitosan microparticles after a calcium silicate treatment. *Acta Biomater.* 2008, 4, 1349–1359.
[149] Thein-Han WW, Kitiyanant Y, Misra RDK. Chitosan as scaffold matrix for tissue engineering. *Mater. Sci. Technol.* 2008, 24, 1062–1075.
[150] Zhou Z, Xiang L, Ou B, Huang T, Zhou H, Zeng W, Liu L, Liu Q, Zhao Y, He S, Huang H. Biological assessment in-vivo of gel-HA scaffold materials containing nano-bioactive glass for tissue engineering. *J. Macromol. Sci. Part A* 2014, 51, 572–576.
[151] Liu Y, Fox V, Lei Y, Hu B, Joo K-I, Wang P. Synthetic niches for differentiation of human embryonic stem cells bypassing embryoid body formation. *J. Biomed. Mater. Res. B Appl. Biomater.* 2014, 102, 1101–1112.
[152] Levenberg S, Huang NF, Lavik E, Rogers AB, Itskovitz-Eldor J, Langer R. Differentiation of human embryonic stem cells on three-dimensional polymer scaffolds. *Proc. Natl. Acad. Sci. USA* 2003, 100, 12741–12746.
[153] Ishaug-Riley SL, Crane-Kruger GM, Yaszemski MJ, Mikos a G. Three-dimensional culture of rat calvarial osteoblasts in porous biodegradable polymers. *Biomaterials* 1998, 19, 1405–1412.
[154] Duan B, Wang M, Zhou WY, Cheung WL, Li ZY, Lu WW. Three-dimensional nanocomposite scaffolds fabricated via selective laser sintering for bone tissue engineering. *Acta Biomater.* 2010, 6, 4495–4505.
[155] Navarro M, Michiardi a, Castaño O, Planell JA. Biomaterials in orthopaedics. *J. R. Soc. Interface* 2008, 5, 1137–1158.
[156] Choi AH, Ben-Nissan B, Conway RC, Macha IJ. Advances in calcium phosphate nanocoatings and nanocomposites. In *Adv. Calcium Phosphate Biomater.*, vol. 2, Ben-Nissan B, Ed. Springer Berlin Heidelberg: Berlin, Heidelberg, 2014.
[157] Zhao L, Chang J. Preparation and characterization of macroporous chitosan/wollastonite composite scaffolds for tissue engineering. *J. Mater. Sci. Mater. Med.* 2004, 15, 625–629.
[158] Peter M, Sudheesh Kumar PT, Binulal NS, Nair SV, Tamura H, Jayakumar R. Development of novel α-chitin/nanobioactive glass ceramic composite scaffolds for tissue engineering applications. *Carbohydr. Polym.* 2009, 78, 926–931.
[159] TenHuisen K, Martin R, Klimkiewicz M, Brown P. Formation and properties of a synthetic bone composite: hydroxyapatite-collagen. *J. Biomed. Mater. Res. Biomed. Mater. Res.* 1995, 29, 803–810.
[160] Scabbia A, Rombelli L. A comparative study on the use of a HA/collagen/chondroitin sulphate biomaterial (Biostite) and a bovine-derived HA xenograft (Bio-Oss) in the treatment of deep intra-osseous defects. *J. Clin. Periodontol.* 2004, 31, 348–355.
[161] Vargas GE, Haro Durand L a, Cadena V, Romero M, Mesones RV, Mačković M, Spallek S, Spiecker E, Boccaccini AR, Gorustovich AA. Effect of nano-sized bioactive glass particles on the angiogenic properties of collagen based composites. *J. Mater. Sci. Mater. Med.* 2013, 24, 1261–1269.
[162] Brandenberg G, Leibrock LG, Shuman R, Malette WG, Quigley H. Chitosan: a new topical hemostatic agent for diffuse capillary bleeding in brain tissue. *Neurosurgery* 1984, 15, 9–13.
[163] Muzzarelli RA, Tanfani F, Emanuelli M, Pace DP, Chiurazzi E, Piani M. Sulfated N-(carboxymethyl)chitosans: novel blood anticoagulants. *Carbohydr. Res.* 1984, 126, 225–231.
[164] Jiang L, Li Y, Wang X, Zhang L, Wen J, Gong M. Preparation and properties of nano-hydroxyapatite/chitosan/carboxymethyl cellulose composite scaffold. *Carbohydr. Polym.* 2008, 74, 680–684.
[165] Tuzlakoglu K, Reis R. Formation of bone-like apatite layer on chitosan fiber mesh scaffolds by a biomimetic spraying process. *J. Mater. Sci.-Mater. Med.* 2007, 18, 1279–1286.
[166] Coutu DL, Yousefi A-M, Galipeau J. Three-dimensional porous scaffolds at the crossroads of tissue engineering and cell-based gene therapy. *J. Cell. Biochem.* 2009, 108, 537–546.
[167] Coutu DL, Cuerquis J, El Ayoubi R, Forner K-A, Roy R, François M, Griffith M, Lillicrap D, Yousefi AM, Blostein MD, Galipeau J. Hierarchical scaffold design for mesenchymal stem cell-based gene therapy of hemophilia B. *Biomaterials* 2011, 32, 295–305.
[168] Baino F, Vitale-Brovarone C. Mechanical properties and reliability of glass–ceramic foam scaffolds for bone repair. *Mater. Lett.* 2014, 118, 27–30.
[169] Gautrot JE, Malmström J, Sundh M, Margadant C, Sonnenberg A, Sutherland DS. The nanoscale geometrical maturation of focal adhesions controls stem cell differentiation and mechanotransduction. *Nano Lett.* 2014, 14, 3945–3952.
[170] Engel E, Michiardi A, Navarro M, Lacroix D, Planell JA. Nanotechnology in regenerative medicine: the materials side. *Trends Biotechnol.* 2008, 26, 39–47.
[171] Supová M. Problem of hydroxyapatite dispersion in polymer matrices: a review. *J. Mater. Sci. Mater. Med.* 2009, 20, 1201–1213.
[172] Lee M, Wu BM. Recent advances in 3D printing of tissue engineering scaffolds. *Methods Mol. Biol.* 2012, 868, 257–267.
[173] El-Ayoubi R, DeGrandpré C, DiRaddo R, Yousefi A-M, Lavigne P. Design and dynamic culture of 3D-scaffolds for

cartilage tissue engineering. *J. Biomater. Appl.* 2011, 25, 429–444.
[174] Yousefi A-M, Gauvin C, Sun L, DiRaddo RW, Fernandes J. Design and fabrication of 3D-plotted polymeric scaffolds in functional tissue engineering. *Polym. Eng. Sci.* 2007, 47, 608–618.
[175] Wei C, Dong J. Direct fabrication of high-resolution three-dimensional polymeric scaffolds using electrohydrodynamic hot jet plotting. *J. Micromech. Microeng.* 2013, 23, 025017.
[176] Lima MJ, Pirraco RP, Sousa R a, Neves NM, Marques a P, Bhattacharya M, Correlo VM, Reis RL. Bottom-up approach to construct microfabricated multi-layer scaffolds for bone tissue engineering. *Biomed. Microdevices* 2014, 16, 69–78.
[177] Martin I, Miot S, Barbero A, Jakob M, Wendt D. Osteochondral tissue engineering. *J. Biomech.* 2007, 40, 750–765.
[178] Yang C, Tibbitt MW, Basta L, Anseth KS. Mechanical memory and dosing influence stem cell fate. *Nat. Mater.* 2014, 13, 645–652.

Amy Yousefi received her PhD in 1996 from the University of Montreal. After a postdoctoral study, she worked at the National Research Council of Canada as a Research Associate from 1999 to 2001 and then as a Research Officer until 2009. Her research at NRC included 3D scaffold design for tissue engineering and cell-based gene therapy, as well as numerical modeling of polymer processing. Since 2009, she has been a Spooner Schallek Associate Professor at Miami University. Her research interests include the design of 3D polymer/bioceramic scaffolds for bone tissue engineering, viscoelastic swelling in 3D-printing, tissue-mimicking phantoms for medical imaging, and finite-element modeling for biomedical applications.

Hassane Oudadesse obtained his PhD in 1989 from the University Blaise Pascal of Clermont-Ferrand in France. He worked as an Associate Professor and obtained his HDR (Habilitation a Diriger des Recherches) in 1998. Since 2001, he has worked as a Full Professor at the Sciences Chimiques, University of Rennes 1 in France. His work concerns the conception, synthesis, and physicochemical studies of new biomaterials for applications in orthopedic surgery, kinetic of bioactivity, kinetic of bioconsolidation in bone-implant interfaces, biocompatibility, cell enhancement, and other properties of biomaterials.

Rosa Akbarzadeh received her MS degree in 2013 from Miami University. After graduation, she worked as a Research Associate on developing 3D-printed polymer/bioceramic scaffolds at Miami University. Her research interests include bone tissue engineering and designing hierarchical scaffolds for biomedical applications.

Eric Wers obtained his Master's degree in Solid State Chemistry and Materials in 2011 from the University of Rennes 1 in France. He is currently a PhD candidate at the University of Rennes 1. His research interests include the elaboration, the physicochemical and biological studies, and the in vivo application of bioactive glasses, porous bioceramics, and chitosan scaffolds for bone tissue engineering. He studied the textural characteristics of biomaterials (size of particles, porosity, and specific surface area), the kinetic of bioactivity by different methods of characterization, the excess entropy, and the release of drug.

Anita Lucas-Girot obtained her PhD from the University of Rennes 1 in France in 1996. In 2002, she joined the University of Rennes 1 as an Assistant Professor. Her research involves bioactive glasses, alumino-silicates, and calcium carbonate-based porous materials for bone substitution.